AD-A100 828   TECHNION - ISRAEL INST OF TECH HAIFA DEPT OF MATERIA--ETC F/G 11/6
THE EFFECT OF HIGH PRESSURE ON PHASE RELATIONSHIPS AND SOME PRO--ETC(U)
MAY 81 A RABINKIN, E GUTMANAS   DA-ERO-78-G-112

UNCLASSIFIED   NL

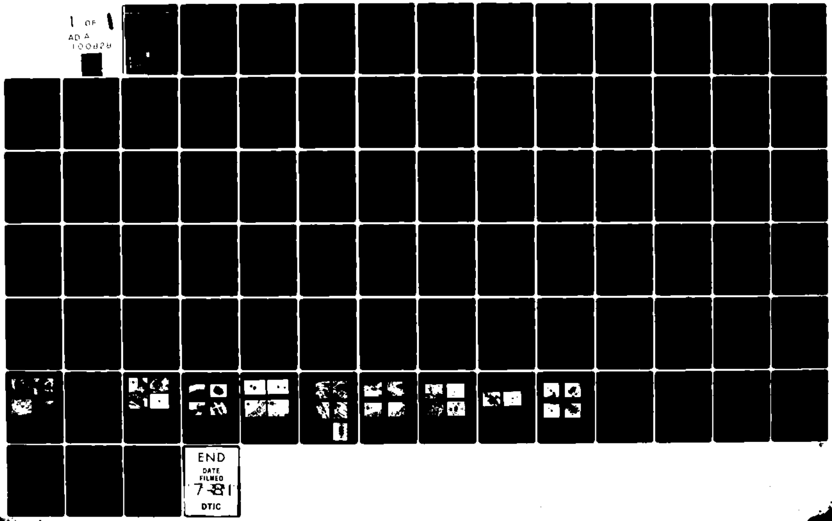

הטכניון — מכון טכנולוגי לישראל   מוסד הטכניון למחקר ופתוח בע"מ
Technion Research & Development Foundation Ltd.   Technion - Israel Institute of Technology

LEVEL II

⑫

המחלקה להנדסת חומרים
DEPARTMENT OF MATERIALS ENGINEERING

LEVEL II ⑫

Grant DAERO-78-G-112

THE EFFECT OF HIGH PRESSURE ON PHASE RELATIONSHIPS AND SOME PROPERTES OF Ti AND ITS ALLOYS

By A. Rabinkin and E. Gutmanas

May 1981
Final Technical Report prepared for

EUROPEAN RESEARCH OFFICE, UNITED STATES ARMY

223 Old Marylebone Road
London NW1 5TH, England

REPORT DOCUMENTATION PAGE		READ INSTRUCTIONS BEFORE COMPLETING FORM
1. Report Number Final Technical Report	2. Govt Acess- AD-A100828	3. Recipient's Catalog Number
4. Title (and Subtitle) The Effect of High Pressure on Phase Relationships and some Properties of Ti and its alloys.		5. Type of Report & Period ~~Covered~~ Final Technical Report Sep[redacted]78 - Jan[redacted]81
		6. Performing Org. Report No.
7. Author(s) Principal Investigator: Prof. A. Rabinkin Investigator : Prof. E. Gutmanas	(10	8. Contract or Grant Number DAERO-78-G-112
9. Performing Organization Name and Address Department of Materials Engineering Technion-Israel Institute of Technology		10. Program Element, Project, Task Area & Work Unit. Nos
11. Controlling Office Name and Address European Research Office, US Army 223 Old Marylebone Road London NW1, 5th, England		12. Report Date (11 May [redacted]81
		13. Number of Pages 82
14. Monitoring Agency Name and Address US Army Procurement Agency Europe, ATTN:AEUPC-PCA 163 Eschersheimer Landstrasse 6000 Frankfurt Main, W. Germany	(12) 79	15. Unclassified

16. & 17. Distribution Statement

Approved for public release; distribution unlimited

18. Supplementary Notes: The work presented in this Report is the subject of four published papers and an additional paper is in preparation. Two additional papers related to this research (Appendix 1 and 2) were published.

19 Key Words

Ti alloys, high pressure, phase transformations

20 Abstract

This report summarizes a research on phase transformations induced by the application of high pressure in Ti, Ti-Mo and Ti-V alloys. The relationship of microstructure, studied by TEM and quantitative X-ray diffraction analysis with mechanical properties and superconductive properties was found.
The effect of alloying and pressurizing on phase stability correlates with changes in basic physical properties of phases.

Form 1473

410 520

Contents

3. Phase transformations in metastable Ti-V and Ti-Mo alloys induced by high pressure treatment.

X

A

Abstract

Changes in crystal structure induced by the application of high pressure up to 9.2 GPa (92 kbar) at 300 K were studied in metastable Ti-Mo and Ti-V alloys in wide concentration range by transmission electron microscopy and were correlated with the results of quantitative X-ray diffraction analysis. The high pressure treatment causes formation of new various structures. The amount of ω phase that remains after the pressure is released is significantly larger than that which is obtained after quenching. As a result of that substantial changes in mechanical properties of the alloys takes place.

Anomalous increasing of the critical temperature to superconductivity T_c was observed in Ti-Mo alloys under pressure. An attempt is made to correlate the effects of alloying and pressurizing on phase stability with changes in basic physical properties of phases.

1. Introduction

It is well known that the structure and properties of solids can be controlled by changing their composition and by thermodynamic parameters such as temperature, pressure (volume) and electromagnetic fields. At present, much data is available on the influences of composition and of temperature on the structure and properties of materials: but due to the many technical difficulties involved, a pressure parameter has not yet been adopted widely for the purpose of influencing structure and properties.

Among many metallic materials Ti and Ti alloys have an increasing industrial significance as constructional and superconductive materials. These materials exist basically in the following crystal structures: β-(b.c.c.), α-h.c.p., α'-h.c.p. martensite and ω-hexagonal. It has been reported that under high static [1-6] and shock pressure [7-10] $\alpha \to \omega$ and $\beta \to \omega$ transformations occur. The presence of the ω phase results in a substantial increase of Young's modulus, tensile strength and hardness [11-13] but it is also accompanied by considerable brittleness. When Ti-alloys are used as superconductors, the appearance of the ω phase during heat treatment results in a remarkable enhancement of the current capacity [14-19] that provides wide possibilities of application in modern technology. The mechanisms of $\beta \to \omega$ and especially $\alpha \to \omega$ transformations are not completely understood. The effect of high pressure on phase equilibria and properties of Ti(Zr) and its alloys is still not sufficiently investigated. For many years only two papers on high pressure induced phase transformation in Ti-alloys are known : one is concerning the Ti-Nb-alloys [20] and the other concerning the Ti-Mo-alloys behaviour after shock loading [9].

The appearance of ω phase in certain Ti alloys is possible since in these materials the thermodynamic characteristics of α, α', β and ω are very similar. Under favourable conditions the existence of the ω phase, at atmospheric pressure, may be energetically more advantageous that either the $\alpha(\alpha')$ or β phases. Such conditions may be created by changing the concentration, pressure (stress field) and temperature. The structures of Ti-alloys are highly sensitive to any changes in the above parameters, which affect strongly their properties.

It is a well accepted idea that there is a certain analogy between the influence of the basic properties of the alloying elements (atomic radii and charge, position in Periodic Chart, etc.) and that of high pressure.

This study tried to solve a few mutually related problems. First, to establish the kind of structural changes induced by the high pressure soaking in β (bcc) isomorphous Ti-based alloys with different initial crystal structures. Second, to compare the influence of both high pressure and alloying on the stability of various metastable phases and mechanical properties of alloys in various structural states. Third, to try to explain the observed regularity between the applied pressure and alloying using the detailed data of the physical properties: Debye temperature, θ_D, Fermi density of states $n(E_F)$, elastic constants etc. The Ti-V and Ti-Mo systems were chosen for the following reasons:

a) In both systems a sequence of metastable phases easily appears upon quenching from the β(bcc) field, and the appearance of any particular structure depends on the Mo or V content. The β isomorphous metastable phase diagram can be subdivided into three regions according to the different phases which can occur. In the first region β(bcc) can transform to a martensitic (α'-hcp or α''-orthorhombic). In the second region β can partially decompose to the omega phase with an hexagonal structure. The β is retained on cooling to room temperature in a region with a higher solute content (Mo>15 at.% and V>20 at.%). At the boundary between the first and the second region, in a narrow range of solute (V and Mo) concentration, a sequence of all these metastable phases α'(or α'') + ω (hexagonal) can appear.

b) Vanadium and molybdenum represent opposite examples of solute elements. In the Periodic Table of elements vanadium is next to titanium : therefore the "rigid band" model of electronic structure can be successfully applied in Ti-V alloys. Molybdenum is located far away from Ti in the Periodic Table and the "rigid band" model is not applicable in this case.

c) The atomic radii of the solute elements (Mo and V) are smaller, therefore their valency electron concentrations are bigger than that of Ti. Alloying of Ti with Mo or V could be regarded analogous to the application of high pressure, since both of them will diminish the mean atomic volume and increase the valence electron concentration n_e. However, there is an important difference in the atomic radius (r_{at}), the number of valency electrons (n_e) and atomic weight (A) of those elements:

$n_e^{Mo}=6$ but $n_e^{V}=5$ ($n_e^{Ti}=4$), $r_{at}^{Mo}=1.39$ Å but $r_{at}^{V}=1.34$ Å ($r_{at}^{Ti}=1.47$), $A^{V}=50.92$, $A^{Mo}=95.94$ ($A^{Ti}=47.90$). Thus the response of Ti-Mo and Ti-V systems to high pressure should be different.

In the Appendix, the data on anomalous behaviour of critical temperature to superconductivity under pressure in Ti-Mo alloys will be reported. This data is very rough and only qualitative analysis will be done taking into account the results on structural changes obtained in previous parts of the present work.

2. Calculations of the metastable diffusionless equilibria in Ti-Mo and Ti-V systems under high pressure conditions [21].

This section presents the results on the construction of the metastable diffusionless equilibria diagrams in the Ti-Mo and Ti-V systems. The regular solution using a thermodynamic approach developed by L. Kaufman will be used [22,23]. For regular solutions the equations for calculating the driving force take the form:

$$\Delta F^{i\to j}_{Ti-Me}[T,P,x] = \Delta F^{i\to j}_{Ti-Me}[T,x] + 23.9P\ \Delta V^{i\to j}[T,P,x] \qquad (1)$$

where $\Delta F^{i\to j}[P,T,x]$ in (cal/g-atom) is the difference in free energy between phase i and j and $\Delta F^{i\to j}[T,x]$ is given by:

$$\Delta F^{i\to j}_{Ti-Me}[T,x] = (1-x)\ \Delta F^{i\to j}_{Ti}[T] + x\Delta F^{i\to j}_{Me}[T] + \Delta F^{i\to j}_{E} \qquad (2)$$

where the Ti concentration in the solid solution is (1-x), the solute (Me) concentration is x and $\Delta F^{i\to j}_E = F^j_E - F^i_E$ is the difference in the free energy of mixing between the i and j phases. The designation i→j can represent transitions between all the metastable phases (α, β, and ω) which occur in Ti-V and Ti-Mo systems.

To compute the diffusionless metastable phase diagrams for these systems under isobaric/isothermal conditions, the free energies of all the metastable phases which exist in both systems must be defined.

In the regular solution model the excess free energy of mixing of the different phases is given by (23):

$$F_E^{\alpha} = x(1-x)\ (A_0 + A_1x + A_2x^2 + --) \qquad (3)$$

$$F_E^{\beta} = x(1-x)\ (B_0 + B_1x + B_2x^2 + --) \qquad (4)$$

$$F_E^{\omega} = x(1-x)\ (W_0 + W_1x + W_2x^2 + --) \qquad (5)$$

In the case at hand an approximation is made by setting:

$$F_E^{\alpha} = x(1-x)A \qquad (6)$$

$$F_E^{\beta} = x(1-x)B \qquad (7)$$

$$F_E^{\omega} = x(1-x)W \qquad (8)$$

where the interaction parameters A, B and W are all temperature independent.

The interaction parameters in the β and ω phases were estimated by Kaufman [22] for Ti-Mo and Ti-V systems using the enthalpies of vaporization, the molar volume and the group numbers of the components. The values of the interaction parameters A and B for the two systems are:

	A (cal/mole)	B (cal/mole)
Ti-Mo	3671	1241
Ti-V	2659	2659

Unfortunately, the value of the interaction parameter W for the ω phase is not known.

By equilibration of partial free energies [23] the interaction parameters A and B can be calculated using the relations

$$\Delta F_{Ti}^{\alpha\to\beta} + RT \ln \frac{1-x_\beta}{1-x_\alpha} = x_\alpha^2 A - x_\beta^2 B \qquad (9)$$

and

$$\Delta F_{Mo}^{\alpha\to\beta} + RT \ln \frac{x_\beta}{x_\alpha})^2 A - (1-x_\beta)^2 B \qquad (10)$$

where x_α and x_β are the atomic fractions of solute Me at the boundaries at a given temperature. To define the dependence of A and B as a function of temperature it is necessary to know the dependence of x_α and x_β as a function of temperature. In the case of Ti-Mo and Ti-V system the value of x_α and x_β are not known very accurately below the 873°C. Moreover the coefficient of A in eq.(9) is small for both systems and this can lead to a large error in solving the equations for thos parameters

The free energy changes accompanying the α→β, β→ω and α→ω transformations in the pure elements [Ti,V,Mo] are given as [22]:

$$\Delta F_{Ti}^{\alpha\to\beta} = 1050 - 0.91\ T \qquad (11)$$

$$\Delta F_{Ti}^{\alpha\to\omega} = 690 - 0.99\ T \qquad (12)$$

$$\Delta F_{Ti}^{\beta\to\omega} = -360 - 0.08\ T \qquad (13)$$

$$\Delta F_{Mo}^{\alpha\to\beta} = -2000\ \text{cal/mole} \qquad (14)$$

$$\Delta F_{V}^{\beta\to\omega} = 1500 + 0.8\ T \qquad (15)$$

The value of $\Delta F_{Mo}^{\beta\to\omega}$ or $\Delta F_{Mo}^{\alpha\to\omega}$ and $\Delta F_{V}^{\beta\to\omega}$ or $\Delta F_{V}^{\alpha\to\omega}$ have not been estimated experimentally or calculated to date. By using equations (1) and (2) in combination with the known value of the differences in the free energy for the pure elements between phases of interest it is possible to compute the P_0-x and T_0-x diagrams under isothermal and isobaric conditions.

Analysis of the m.d.e. diagrams (metastable diffusionless equilibria diagrams) can be performed by noting that the T_o-x and P_o-x lines do not show the actual value of the temperature or pressure at which the given alloy undergoes transformations. These curves correspond to $\Delta F^{i\to j} = 0$. As an approximation T_o and/or P_o is taken to be the average between the forward and reverse transformations. Therefore, experimentally T_0 is usually estimated as

$T_0 = 1/2\ [M_S^{i\to j} + A_S^{j\to i}]$ and $P_0 = 1/2\ [P_S^{i\to j} + P_S^{j\to i}]$

In the Ti-Mo system the free energy equations have the form:

$$\Delta F^{\beta\to\alpha} = (1-x)\ (-1050+0.91T) + 2000\ x + x(1-x)\ [A-B] + 23.9P\ \Delta V^{\beta\to\alpha} \qquad (16)$$

$$\Delta F^{\beta\to\omega} = (1-x)\ (-690+0.99T) + x\Delta F_{Mo}^{\beta\to\omega} + x(1-x)\ [W-B] + 23.9P\ \Delta V^{\beta\to\omega} \qquad (17)$$

$$\Delta F^{\alpha\to\omega} = (1-x)\ (360+0.08T) + x\Delta F_{Mo}^{\alpha\to\omega} + x(1-x)[W-A] + 23.9P\ \Delta V^{\alpha\to\omega} \qquad (18)$$

Substitution of the interaction parameters A and B estimated by Kautman into eq. 16 at $T_0^{\beta\to\alpha} = 300K$ yields a value of x = 0.16 for the atomic fraction of Mo where ΔF = 0. Alternatively one can use eqs. 9 and 10 to recalculate A and B taking into account that for the Ti-Mo system x_α and x_β are well known [24] at T = 9[illegible]3 K ($x_\alpha = 0.003$ and $x_\beta = 0.11$). This yields the interaction parameter values A = 7500 cal/g. atom and B = 3100 cal/g. atom which are more positive than those previously estimated [22]. Substitution of these values in eq. 16 at $T_0 = 300K$ yields x = 0.11 which is a more acceptable value for the ΔF T_0 vs. x curve and in better accordance with M_d experimental data [25]. These parameters fix the form of $\Delta F^{\beta\to\alpha}[T,x]$ at atmospheric pressure as,

$$\Delta F^{\beta\rightarrow\alpha}[T,x] = (1-x)[-1050+0.91T] + 2000x + x(1-x)[7500-3100] \qquad (19)$$

or for low concentration i.e. where $x(1-x)\rightarrow x$

$$\Delta F^{\beta\rightarrow\alpha}[T,x] = (1-x)(-1050+0.91T) + 6400x \text{ cal/g.atom} \qquad (20)$$

At atmospheric pressure the free energy difference equations for the $\beta\rightarrow\omega$ transition is given by:

$$\Delta F^{\beta\rightarrow\omega}[T,x] = (1-x)(-690+0.99T) + x\,\Delta F_{Mo}^{\beta\rightarrow\omega} + [W-B]\,x\,(1-x)$$

at low solute levels $x(1-x)\rightarrow x$ yielding:

$$\Delta F^{\beta\rightarrow\omega}[T,x] = (1-x)(-690+0.99T) + x[\Delta F_{Mo}^{\beta\rightarrow\omega}+W-B] \qquad (21)$$

Since the one atmosphere, T_0 = 300K, upper limit for $\beta\rightarrow\omega$ transition occurs at x=16-17 at% Mo (13,14) then setting the driving force $\Delta F^{\beta\rightarrow\omega}[T,x] = 0$ under these conditions yields

$$\Delta F_{Mo}^{\beta\rightarrow\omega} + [W-B] = 2000 \text{ cal/g.atom} \qquad (22)$$

With this assumption

$$\Delta F^{\beta\rightarrow\omega}[T,x] = (1-x)[-690+0.99T] + 2000x \text{ cal/g.atom} \qquad (23)$$

The driving force for $\alpha\rightarrow\omega$ transition can be directly obtained by subtracting eq. (2) from (23) yielding

$$\Delta F^{\alpha\rightarrow\omega}[T,x] = (1-x)(360+0.08T) - 4400X \text{ cal/g.atom} \qquad (24)$$

Equations (20), (23) and (24) which describe the one atmosphere relative stability of α, β and ω phases for diffusionless transformations can be used to compute the T_0-x diagram at atmospheric pressure. This T_0-x diagram for the Ti-Mo system is shown in Fig.1. The dashed region in this diagram represents the region of the metastable ω phase.

In order to calculate the P_0-x metastable diagram T_0 = 300K the values of $\Delta V^{i\rightarrow j}(P,x)$ the difference in the molar volume between α,β or ω phase pairs as a function of pressure and solute concentration must be known. The dependence of V^{α}, V^{β}, V^{ω} as a function of the applied pressure was not measured experimentally

$$\Delta F^{\beta\to\alpha}[T,x] = (1-x)[-1050+0.91T] + 2000x + x(1-x)[7500-3100] \qquad (19)$$

or for low concentration i.e. where $x(1-x)\to x$

$$\Delta F^{\beta\to\alpha}[T,x] = (1-x)(-1050+0.91T) + 6400x \text{ cal/g.atom} \qquad (20)$$

At atmospheric pressure the free energy difference equations for the $\beta\to\omega$ transition is given by:

$$\Delta F^{\beta\to\omega}[T,x] = (1-x)(-690+0.99T) + x\,\Delta F^{\beta\to\omega}_{Mo} + [W-B]\,x\,(1-x)$$

at low solute levels $x(1-x)\to x$ yielding:

$$\Delta F^{\beta\to\omega}[T,x] = (1-x)(-690+0.99T) + x[\Delta F^{\beta\to\omega}_{Mo}+W-B] \qquad (21)$$

Since the one atmosphere, T_0 = 300K, upper limit for $\beta\to\omega$ transition occurs at x=16-17 at% Mo (13,14) then setting the driving force $\Delta F^{\beta\to\omega}[T,x] = 0$ under these conditions yields

$$\Delta F^{\beta\to\omega}_{Mo} + [W-B] = 2000 \text{ cal/g.atom} \qquad (22)$$

With this assumption

$$\Delta F^{\beta\to\omega}[T,x] = (1-x)[-690+0.99T] + 2000x \text{ cal/g.atom} \qquad (23)$$

The driving force for $\alpha\to\omega$ transition can be directly obtained by subtracting eq. (2) from (23) yielding

$$\Delta F^{\alpha\to\omega}[T,x] = (1-x)(360+0.08T) - 4400X \text{ cal/g.atom} \qquad (24)$$

Equations (20), (23) and (24) which describe the one atmosphere relative stability of α, β and ω phases for diffusionless transformations can be used to compute the T_0-x diagram at atmospheric pressure. This T_0-x diagram for the Ti-Mo system is shown in Fig.1. The dashed region in this diagram represents the region of the metastable ω phase.

In order to calculate the P_0-x metastable diagram T_0 = 300K the values of $\Delta V^{i\to j}(P,x)$ the difference in the molar volume between α,β or ω phase pairs as a function of pressure and solute concentration must be known. The dependence of V^{α}, V^{β}, V^{ω} as a function of the applied pressure was not measured experimentally but can be estimated using the elastic moduli data for Ti-Mo and Ti-V alloys provided by Fedotov [14,26,27]. The elastic modulus of "pure" ω phase was estimated by Bowen from strain-deformation relationship measurements [27]. The dependence of volume of pure α-Ti on applied pressure was given by Fisher et al. [28] with use of the Murnagham's equation for α-Ti which is as follows:

$$\frac{V^{\alpha}[P]}{V^{\alpha}[0]} = [1+0.0040923\ P]^{-0.22978} \tag{25}$$

which can also be expressed in P power series as:

$$V^{\alpha}[P] = V^{\alpha}[0]\ [1-0.93\ 10^{-3}P + 2.51\ 10^{-6}P^{2}] \tag{26}$$

where $V^{\alpha}[0]$ is the volume of hcp Ti at 300K and one atmosphere. The compressibility obtained from eq. (26) is equal to 0.93×10^{-3}. This compares well with the compressibility of 1.03×10^{-3} calculated from the relations between bulk modulus, the elastic modulus and the Poisson ratio.

The dependence of V^{ω} on pressure is estimated to be:

$$V^{\omega}[P] = V^{\omega}[0][1-0.69\ 10^{-3}P + 6.52\ 10^{-7}P^{2}] \tag{27}$$

where $V^{\omega}[0]$ is the volume of the pure ω titanium at 300K and one atmosphere. This equation was developed by using experimental data [29] for ω zirconium. The calculated and experimental pressure dependences of V^{α}, V^{β} and V^{ω} are shown in Fig. 2

Since $\Delta V^{\alpha\to\omega}$ for titanium is a moderate function of pressure the main charge in $\Delta V^{\alpha\to\omega}$ on alloying is due to concentration. The experimental values of the molar volume of the different phases α, β, or ω which exist in the Ti-V and Ti-Mo systems taken from different sources including present research data is given in Fig. 3.

For the Ti-Mo system:

$$V^{\omega}[x] = V^{\omega}[0]\ (1-0.152x)\ \mathrm{cm}^3/\mathrm{g.at.} \qquad (28)$$

$$V^{\beta}[x] = V^{\beta}[0]\ (1-0.180x) \qquad (29)$$

$$V^{\alpha}[x] = V^{\alpha}[0]\ (1-0.302x) \qquad (30)$$

For the Ti-V system:

$$V^{\omega}[x] = V^{\omega}[0]\ (1-0.141x);\ V^{\omega}[0] = 10.47 \qquad (31)$$

$$V^{\beta}[x] = V^{\beta}[0]\ (1-0.157x);\ V^{\beta}[0] = 10.60 \qquad (32)$$

$$V^{\alpha}[x] = V^{\alpha}[0]\ (1-0.214x);\ V^{\alpha}[0] = 10.66 \qquad (33)$$

Under these conditions the dependence of $\Delta V^{i\to j}$ for α,β and ω phases can be calculated as a function of the solute content. Finally, the relative stability of the metastable α, β and ω phases in Ti-Mo system at T = 300K is given by equations (34-36).

$$\Delta F^{\beta\to\alpha}[T=300K,P,x] = (1-x)(-777) + 6400x + 23.9P\ \Delta V^{\beta\to\alpha}[x,P] \qquad (34)$$

$$\Delta F^{\beta\to\omega}[T=300K,P,x] = (1-x)(-393) + 2000x + 23.9P\ \Delta V^{\beta\to\omega}[x,P] \qquad (35)$$

$$\Delta F^{\alpha\to\omega}[T=300K,P,x] = (1-x)(384) - 4400x + 23.9P\ \Delta V^{\alpha\to\omega}[x,P] \qquad (36)$$

which are derived by substitution of equations 20, 23, 24 and 28-33 into equation 1. The computed P_0-x metastable diffusionless phase diagram based on equations (34) and *36) is presented in Fig.4 together with the experimental data on different phases observed under pressure in Ti-Mo system.

The same regular solution approach can be used to calculate $\Delta F^{i\to j}$ equations for Ti-V alloys.

The free energy difference for $\beta\to\alpha$ transition is given generally in Ti-V system at atmospheric pressure by:

$$\Delta F^{\beta\to\alpha}\ [T,x] = (1-x)\ \Delta F^{\beta\to\alpha}_{Ti} + x\Delta F^{\beta\to\alpha}_{V} + x(1-x)\ (A-B)\ \mathrm{cal/g.\ atom.} \qquad (37)$$

or introducing the value of $\Delta F^{\beta\to\alpha}_{Ti}$ and $\Delta F^{\beta\to\alpha}_{V}$:

$$\Delta F^{\beta\to\alpha}\ [T,x] = (1-x)\ (-1050 + 0.91T) + x\ (1500 + 0.8T) + (1-x)\ (A-B)\ \mathrm{cal/g.\ atm.} \qquad (38)$$

Using the Kaufman calculated mixing energy parameters A and B for Ti-V in equation (38) one obtains $\Delta F^{\beta\to\alpha}$ [T,x] = 0 at x = 31 at.% V at 300K. But, as follows from the experimental data in [30], unfortunately these parameters cannot describe properly the low temperature region of T-x phase diagrams in Ti-V systems. Namely, the use of Kaufman mixing energy parameters A and B, independent of temperature, do not agree with experimental data in the concentration region where ω phase exists upon quenching. (For the Ti-Mo system the simplification in A and B temperature independence has no substantial meaning since $T_0^{\beta\to\alpha}$ in that system has strong concentration dependence. Therefore a possible mistake in location of $T_0^{\beta\to\alpha}$ is a small one). For proper description and good fitting with the experimental data obtained, it is necessary to have a temperature dependence of the mixing energy parameters A and B. As in the case of Ti-Mo system, it is not possible to evaluate the temperature dependence of A and B separately because of lack of exact data needed for use of eq. (9) and (10) over the temperature range. In these conditions, to calculate the temperature dependence of (A-B), the widely accepted approximation (31,23,32) was invoked, that the difference between $M_S^{\alpha'\to\beta}$ and $T_0^{\alpha'\to\beta}$ is not large i.e. that the corresponding chemical driving force for the martensitic transformation $\alpha'\to\beta$ in the Ti-β stabilizer alloys, $\Delta F^{\beta\to\alpha}|M_s$ is about - (50-60) cal/mole. In the same way, because the strain energy associated with the diffusionless $\beta\to\omega$ transformation is even smaller than at $\beta\to\omega$, the $T_0^{\beta\to\omega}$ can be taken from corrected data on $M_s^{\beta\to\omega}$ [32]. Therefore by use of Duwez's data on temperature dependence of $M_s^{\alpha'\to\beta}$ in Ti-V alloys [32] with the above mentioned correction for $\Delta F^{\beta\to\alpha'}$, the expression for (A-B) can be obtained finally from eq. (38) as follows:

(A-B) = 5180 - 505T for Ti-V

Now, with the knowledge of temperature dependence of (A-B), it is now possible to calculate full concentration dependence of $T_0^{\beta\to\alpha}$. By substituting the temperature dependence of (A-B) eq. 38 becomes:

$$\Delta F^{\beta\to\alpha}[T,x] = (1-x)(-1050+0.91T) + x(1500+0.8T) + x(1-x)\ (5190-5.5T)\ \text{cal/g.atom} \qquad (39)$$

For β→ω transformation the free energy difference is given by:

$$\Delta F^{\beta\to\omega}\ [T,x] = (1-x)\ (-690+0.99T) + x\ \Delta F_V^{\beta\to\omega} + x[W-B]\ (1-x)\ \text{cal/g.atom} \qquad (40)$$

in the limit where $x(1-x)\to x$

$$\Delta F^{\beta\to\omega}[T,x] = (1-x)\ (-690+0.99T) + x\ [\Delta F_V^{\beta\to\omega} + W-B] \qquad (41)$$

The highest vanadium concentration observed for β→ω diffusionless transformation at 300K is 25 at.% V [30,34], i.e. $M_s^{\beta\to\omega} = 300$ K. From $\Delta F^{\beta\to\omega}\ [T,x] = 0$ in eq. (41) it yields that at 300K and $x = 0.25$

$$1180 = \Delta F_V^{\beta\to\omega} + W-B \qquad (42)$$

$$\Delta F^{\beta\to\omega}\ [T,x] = (1-x)\ (-690+0.99T) + 118-x \qquad (43)$$

Subtraction of eq. 39 from eq. 43 yields:

$$\Delta F^{\alpha\to\omega}\ [T,x] = (1-x)(360+0.08T) - x(320+0.8T) - x(1-x)(5180-5.5T) \qquad (44)$$

The combination of equations (39), (43) and (44) describe the T_0-x diagrams for the stable and metastable α,β and ω phases which occur in the Ti-V system at atmospheric pressure, when no diffusion occurs under these conditions. This expression does not change practically Kaufman's description of T-x phase diagrams of Ti-base alloys at higher temperature. In the same time there is much better accordance now between calculated data and experimental results on the phases present upon quench and successive phase transformation under pressure. The boundaries are established by the use of conditions $\Delta F^{i\to j}\ [T,x] = 0$. The calculated T_0,x diagram for Ti-V system is presented in Fig.5 where the hatched area is the range of ω stability in this system.

To calculate the P_0-x diagram, the extended free energy equations are employed which include the dependence of $\Delta F^{i\to j}$ on temperature, pressure and concentration.

The free energy equations at the isothermal condition (T=300K) are given by:

$$\Delta F^{\beta\to\alpha}\,[T,P,x] = (1-x)(-1050+0.91T) + x(1500+0.8T) + x(1-x)(5180-5.5T) + 23.9P\,\Delta V^{\beta\to\alpha}\,[P,x]\ \text{cal/g. atom} \qquad (45)$$

$$\Delta F^{\beta\to\omega}\,[T,P,x] = (1-x)(-630+0.99T) + 1180x + 23.9P\,\Delta F^{\beta\to\omega}_{Ti-V}\,[P,x] \qquad (46)$$

$$\Delta F^{\alpha\to\omega}\,[T,P,x] = (1-x)\,(360+0.08T) - x(320+0.8T) - x(1-x)\,(5180-5.5T) + 23.9P\,\Delta V^{\alpha\to\omega}\,[P,x]\ \text{cal/g. atom} \qquad (47)$$

Since the pressure dependence of $\Delta V^{\alpha\to\omega}$ for pure Ti is small we assume that $\Delta V^{i\to j}$ for the Ti-V system is a function of solute concentration only. The experimental data on V^i $(i=\alpha,\beta,\omega)$ as a function of solute concentration x in Ti-V alloys is given by equations (31,33). Substitution into equations (45-47) results in equations which describe the diffusionless P_0-x diagram at T = 300K. The pressure dependence P_0 on x is given by the condition $\Delta F^{i\to j}$ [T=300K,P,x] = 0. The computed P_0-x diagram at T = 300K for the Ti-V system is shown in Fig. 6 together with the experimental results on the stability of different phases which occur in this system under high pressure (see next section).

3. Phase transformations in metastable Ti-V and Ti-Mo alloys induced by high pressure treatment

This section presents the experimental results on structural changes in Ti-V and Ti-Mo. Only the metastable structures created by quenching were pressurized and high pressure was applied at room temperature. Therefore, all observed phase transformations were regarded as completely diffusionless. It should be noted that in most of the previous publications, for example, [35-37], the phase transformations in metastable Ti-alloys were diffusion-controlled.

The choice of the alloys' concentration was done in such a way that all the main as-quenched structures in Ti alloys, i.e. α', $\alpha'+\omega+\beta$, $\beta+\omega$ and β could be investigated.

3.1. Experimental procedure

a) Sample preparation

The alloys were arc melted from titanium (>99.9 wt.% analytical purity) with V or Mo (both spectroscopical purity) on water-cooled cold hearth and remelted 5 times to insure homogeneity. A protective atmosphere of purified argon and a titanium getter was used. The weight changes, after melting, were small ($\lesssim$ 0.1%) and the composition of the alloys was calculated from the weight of components. The resultant ingots were cut into plates which were cold rolled to foils of 100-120 μm thickness. The specimens for structural studies were annealed 3h at 1100°C in a furnace with a dynamic vacuum, better than 2.10^{-6} torr and then quenched under vacuum into DC 704 diffusion pump fluid. The composition of the samples of the alloys is shown in Tables 1 and 2 together with the lattice parameters and the phase content.*

b) High pressure treatment

The high pressure treatment was carried out on a single stage apparatus with a solid-medium cell providing the minimal deviation (1-2%) from uniformity. The pressure mediums were graphite and AgCl. The pressure inside a pyrophilite cell was calibrated by tracing the phase transitions of BiI-BiII (2.54 GPa), BaI-BaII (5.5 GPa), BiIII-BiV (7.60 GPa) and SnI-SnII (9.2 GPa). The samples, in the shape of disks, were placed inside a cell. Pressure was increased at a rate less than 1 MPa/min up to a specified value. This pressure was maintained for 2 to 24 hours with subsequent releasing of pressure for 1 hour. After such a procedure all samples were subjected to structural analysis.

---

* The Mo and V concentration will be given in atomic percent throughout.

c) X-ray and electron microscopy analysis

X-ray diffraction patterns were taken using a Phillips diffractometer with CuKα radiation equipped with a bent single crystal graphite monochromator. The volume percent of ω-phase was determined from the relative integrated intensities of α,β and ω-reflections. The structure factors, Lorentz polarization factors and unit cell size of the ω,β and α phases were taken from [38-40]. It was assumed that the temperature factor for β,α and ω phases was of a similar magnitude. The error in the volume fraction calculation was approximately ± 3 vol. pct.

The electron microscope samples were electropolished at -40°C under conditions proposed by Blackburn and Williams [41]. The structures were examined using both JEOL 100B and JEOL 200B electron microscopes at 100 kv and 150 kv respectively.

3.2. Experimental results

a) Ti-Mo system

Ti.3% Mo

In the as-quenched state, X-ray analysis reveals the existence of two martensitic phases: α' with an hcp structure and α" with an orthorhombic structure described previously [42-44]. (X-ray analysis data for all alloys is presented in Table 1). The micrograph in fig. 7a illustrates the complex martensitic structure of the as-quenched Ti-3 Mo alloy. α' fine plates are seen in region A (see Fig.7a) big plates of α' martensite (B) divide the bulk of what seems to be α" martensite. Retained β phase was not detected after quenching.

After hps at 4.5 GPa for 3 h no significant changes in the quenched structure could be seen by TEM examination and on X-ray diffractograms.

After hps at 7.5 GPa for 3 h very small particles of the second phase were observed with a highly densed dislocation network in the α' martensite plates (see fig. 7b). The experiment on measurement of sample resistivity under high pressure showed a moderate but definite change in the resistivity of the sample at $P = 7.0$ GPa. This can certainly be attributed to the onset of ω phase formation.

After hps at 9.2 GPa the volume fraction of ω phase approached 23% as judged by X-ray analysis. The structure of the soaked alloy is shown in figs. 7c,d. The contrast of the ω particles appeared only under certain diffraction conditions. The morphology of the induced particles imaged in the dark-field (fig. 7) was difficult to distinguish.

Ti-5% Mo

In the as quenched state X-ray analysis (fig. 8a) and TEM (fig. 9a) showed that the structure consisted of the following three phases: α-martensite in the shape of small needles, and a β-matrix in which very small ω particles are embedded. The electron diffraction pattern (see fig. 9a) confirms the presence of ω phase. X-ray diffraction obtained from bulk sample showed that the type of martensite (α'') in this alloy has an orthorhombic structure as it was identified by the pair of high angle lines (200) α'' and (130) α''. An insufficient small separation between the low angle lines (110) α'' and (1020) α'' and (021) α'' and (111) α'' makes the differentiation between a hexagonal and and orthorhombic product more difficult in this case. Furthermore, electron microscopy examination of thin foils prepared from the same sample used for X-ray diffraction shows evidence of a distorted hexagonal martensite.

After hps at 7.0 GPa and especially 9.0 GPa the quantity of α and ω phases increased as determined by X-ray data (fig. 8a). The structure of this alloy subjected to hps 7.0 GPa is shown in fig. 9b. It can be observed that pressure-induced α-martensite plates grow at the expense of the β-matrix.

An increase of hps up to 9.0 GPa gave rise to the enlargement of α'-martensite plates (see fig. 9c). The large α'plates contain a mixture of $\omega + \beta$ (possibly as a result of partial transformation of α' to $\omega + \beta$), as well as "secondary" α' plate-like regions. Superimposed reciprocal lattice sections of ω,β and α' phases are seen in the diffraction pattern and in the corresponding indexing scheme (see figs. 9d,e). This complex structure may be the result of the similarity of the thermodynamic properties of all three phases in this particular alloy. Therefore, the application of high pressure causes successive stages in phase transformation development. This development could also proceed in a reverse direction during the unloading of the sample.

Ti-11.5% Mo

In the as-quenched state the X-ray diffractograms (fig. 8b) showed no traces of ω phase. On the other hand, the TEM micrograph exhibited a mottled contrast, which can be attributed to a finely dispersed phase. This dispersive phase or, more correctly, the small zones which may serve as precursors for ω phase are probably responsible for the small degree of diffuse streaking observed on the corresponding diffraction pattern.

After hps at 9.2 GPa the quantity of ω induced phase was evaluated by X-ray diffraction analysis (see fig. 8b) as $\sim$ 15 vol.%. Application of pressure gave rise to dislocation network and growth of the second phase particles. The electron diffraction pattern shows clear reflections of ω particles and circular diffuse streaks. Diffraction of distinct ω particles results in appearance of clear ω reflections. While the increasing amount of the ω phase precursors are responsible for the marked diffuse streaking. The dislocation network observed after hps is due to the increasing transformation strains, and compression strains created by pressurization of samples with a structure containing a mixture of anisotropic phases.

Ti-15% Mo

In the as-quenched state the "athermal" ω phase was easily imaged in the extinction contours (see fig. 10a). This can be explained by the dynamic diffraction conditions inside the extinction contours providing the best contrast for very small coherent particles. The extinction countours themselves could be local distortions in the β-matrix caused by the transformation strains The electron diffraction pattern shows a complex network of diffuse intensity (see fig. 10b). The paired positions of ω spots reflect the symmetrical arrangement of the ω precipitates to each other relative to {110} plane.

After hps at 9.0 GPa the quantity of the ω phase increased. The grown ω phase particles appear together with a dislocation network as is shown in fig. 10c.

Ti with 18 to 35% Mo

In the as-quenched state the X-ray analysis of all these alloys revealed the existence of only one phase (identified as the β-phase). Diffuse scattering was observed on the electron diffraction pattern of the as-quenched Ti-18% Mo alloy (see fig. 11a) and paired Kikuchi lines appeared on the electron diffraction pattern of the Ti-20% Mo alloy (see fig. 11b). It is interesting to note that the composition of these alloys corresponds to the maximum of the miscibility gap of the Ti-Mo phase diagram [47] The effect of diffuse scattering and paired Kikuchi lines is usually assigned to the first stages of spinodal decomposition. But it is difficult to suggest that such decomposition could occur during the quick quench of these alloys It is more likely that the formation of short range ordered zones due to the static displacements of short atomic rows resulted in the observed effects [45]. No peculiar details were observed for as-quenched Ti-25% Mo alloy in the TEM micrographs

After hps at 4.5 GPa the TEM examination revealed particles of a second phase in alloys containing 18 to 25% Mo (see figs. 11c,d) These particles have an ellipsoidal shape characteristic of the ω phase. However, analysis of the diffraction pattern did not allow these particles to be identified as ω phase. Probably the structure of the pressure induced phase is distorted and its crystallographic structure is different from the "classical" ω phase

This distortion of ω phase can be caused by its elastic interaction with a β-matrix, possessing significantly more rigidity in comparison with alloys containing less Mo. The alternative reason might be the decrease of the ω phase symmetry due to the increase of a pair interaction between Mo atoms in these alloys with a large amount of molybdenum.

X-ray analysis in all samples showed no trace of ω phase lines, and the quantity of ω phase may be evaluated as less than 2 to 3%.

After hps at 9.0 GPa, no change was obtained in the X-ray diffractograms which showed only lines characteristic of the β phase.

The results of phase content analysis and lattice parameter determination are summarized in Table I. Fig.3 shows the variation of molar volumes for α, β and ω phases as a function of composition. The data of X-ray analysis are in accordance with TEM observation. It shows that the ω phase remains in substantial quantity after a high pressure release.

From the data presented in Table I, it follows that the specific volume V^{α} for α phase depends on the molybdenum content more than the specific volume V^{β} does for β phase (see fig. 3). Therefore for alloys with Mo > 5% specific volume increment $\Delta V^{\beta\to\alpha}$ becomes negative ($\Delta V^{\beta\to\alpha} < 0$). That means that the high pressure will provide a driving force $\Delta V \times \Delta P$ for both $\beta\to\omega$ transformation ($\Delta V^{\beta\to\omega} < 0$ for all concentration range) when Mo > 5%

b) Ti-V system

Ti-2% V, Ti-6% V alloys

X-ray analysis of the quenched Ti-2% V and Ti-6% V alloys indicated that only hexagonal α' martensitic phase was present and it was confirmed by electron microscopy (see Table II).

When pressurizing the samples at 6.5 GPa and 9.2 GPa the electrical resistivity was measured. No step-like changes in the electrical resistivity

Table 1: The phase content and lattice parameters of Ti-Mo alloys after quenching and high pressure soaking at room temperature

Sample Content (at.%)	Phases present	Volume fraction	Experimental lattice parameters (Å) (± 0.006)	Specific volume (cm^3/mol)	Phases present	Volume fraction	Experimental lattice parameters (Å) (± 0.006)	Specific volume⁺ of ω phase (cm^3/mol)
		After quenching				After high pressure soaking up to 9.0 GPa		
$Ti_{97}Mo_3$	α' (hcp)	0.35	α' $a = 2.954$ $c = 4.650$	10.57	α'	0.28		
	α" (ortho)	0.65	α" $a = 3.007$ $b = 5.021$ $c = 4.650$	10.54	α" ω	0.49 0.23	$a_\omega = 4.612$ $c_\omega = 2.821$	10.42
$Ti_{95}Mo_5$	α" (ortho) β (bcc) ω (hex)	0.21 0.58 0.21	$a_\beta = 3.280$	10.62	α" β ω	0.36 0.23 0.41	$a_\omega = 4.602$ $c_\omega = 2.820$	10.37
$Ti_{88.5}Mo_{11.5}$	β (bcc) ω*	0.15-1**	$a_\beta = 3.251$	10.35	β ω	0.84 0.16	$a_\omega = 4.591$ $c_\omega = 2.815$	10.31
$Ti_{85}Mo_{15}$	β ω*	0.9-1**	$a_\beta = 3.247$	10.30	β⁺⁺ ω*	0.9-1	$a_\omega = 4.587$ $c_\omega = 2.808$	10.23
$Ti_{82}Mo_{18}$	β	1	$a_\beta = 3.243$	10.27	β⁺⁺ ω*	0.9-1		
$Ti_{75}Mo_{25}$	β	1	$a_\beta = 3.229$	10.14	β⁺⁺ ω*	0.9-1		

* Phase detected by electron microscope analysis.

** X-ray analysis doesn't reveal the existence of ω phase

\+ According to expression $V_{\alpha'} = \sqrt{3}a^2c/4 \cdot 6.02 \cdot 10^{23}$ cm^3/mol; $V_\beta = a^3/2 \cdot 6.02 \cdot 10^{23}$ cm^3/mol; $V_{\alpha''} = abc/4 \cdot 6.02 \cdot 10^{23}$ cm^3/mol; $V_\omega = \sqrt{3}a^2c/6 \cdot 6.02 \cdot 10^{23}$ cm^3/mol

++ The sample was soaked up to 4.5 GPa

Table 2: The phase content and lattice parameters of Ti-V alloys after quenching and high pressure soaking at room temperature

Sample content (%)	Phases present	Volume fraction (%)	Experimental lattice parameters (Å) (±0.006)	Specific volume (cm^3/mole)	Phases present	Volume fraction (%)	Experimental lattice of ω phase (Å) (±0.006)	Specific vol. of ω phase (cm^3/mole)	c/a value of ω phase
	After quenching				After high pressure soaking up to 9.0 GPa				
Ti-2V	α' (hcp)	$V_{\alpha'}=100$	$a = 2.949$ $c = 4.686$	$V_{\alpha'}=10.63$	α'	100	-	-	ω-Ti (0.610*)
Ti-6V	α' (hcp)	$V_{\alpha'}=100$	$a = 2.942$ $c = 4.678$	$V_{\alpha'}=10.56$	α' ω	$V_{\alpha'}=64$ $V_\omega=36$	$a_\omega=4.604$ $c_\omega=2.819$	$V_\omega=10.38$	0.6112
Ti-10V	α' (hcp) β (bcc) ω (hex)	$V_{\alpha'}=44$ $V_\beta=34$ $V_\omega=22$	$a_{\alpha'}=2.936$ $c_{\alpha'}=4.667$ $a_\beta=3.261$	$V_{\alpha'}=10.48$ $V_\beta=10.44$	α' β ω	$V_\alpha=31$ $V_\beta=26$ $V_\omega=43$	$a_\omega=4.594$ $c_\omega=2.813$	$V_\omega=10.32$	0.6123
Ti-14V	β (bcc) ω (hex)	$V_\beta=68$ $V_\omega=32$	$a_\beta=3.254$	$V_\beta=10.38$	β ω α'	$V_\beta=38$ $V_\omega=57$ $V_{\alpha'}<5$	$a_\omega=4.586$ $c_\omega=2.810$	$V_\omega=10.28$	0.6127
Ti-20V	β (bcc) ω (traces)	$V_\beta=90-100$	$a_\beta=3.238$	$V_\beta=10.26$	β ω α' (traces)	$V_\beta=74$ $V_\omega=26$	$a_\omega=4.573$ $c_\omega=2.804$	$V_\omega=10.19$	0.6132
Ti-30V	β (bcc)	$V_\beta=100$	$a_\beta=3.227$	$V_\beta=10.11$	β	$V_\beta=100$	-	-	
Ti-35V	β (bcc)	$V_\beta=100$	$a_\beta=3.217$	$V_\beta=10.02$	β	$V_\beta=100$	-	-	
Ti-40	β (bcc)	$V_\beta=100$	$a_\beta=3.210$	$V_\beta=9.96$	β	$V_\beta=100$	-	-	

+ acording to expression $V_{\alpha'} = \sqrt{3}\, a^2 c/4 \times 6.02\cdot 10^{23}\, cm^3/mole$; $V_\omega = \sqrt{3}\, a^2 c/6 \cdot 6.02\cdot 10^{23}\, cm^3/mole$

$$V_\beta = a^3/_2 \cdot 6.02\cdot 10^{23}\, cm^3/mole.$$

* according to Jamieson data for pure ω-Ti [16].

were found in the case of Ti-2% V, but distinct change in the slope of the resistivity-pressure curve for Ti-6 %V was observed. This fact was regarded as the evidence of the ω phase formation in Ti-6% alloy under high pressure. On the other hand the extensive examination by electron transmission microscopy (TEM) failed to reveal the presence of the ω phase in Ti-6% V specimens after a high pressure run.

It is possible that the pressure formed ω-phase was destroyed and transformed back to α' martensite after releasing the pressure. Only martensitic plates of titanium α' - martensite with acicular morphology were observed (fig.12).

Ti-10% V alloy

α' - martensite, β-phase and athermal ω-phase were found in quenched specimens by means of an X-ray technique. Electron micrography taken from these specimens show α' martensitic plates in β matrix and very fine thin ω plates inside an α' martensitic plate. Fig. 13a represents the morphology of these thin ω plates in the dark field taken from the ω-reflection. Corresponding electron diffraction pattern and its schematic representation are given in fig. 13c and fig. 13d. The analysis of this electron diffraction pattern shows that the orientation relations of α' and ω plates to the β phase are consistent with those usually observed for β→α and β→ω transformation [46]. Small ellipsoidal ω particles were also observed in β matrix and the well known ω/β orientation relationships [46], were confirmed. It should be pointed out that it is not clear whether the ω particles observed in α' martensitic plate are the result of direct α→ω transition or whether both β→α' and β→ω transformations have taken place simultaneously.

After high pressure soaking at 9.2 GPa the amount of the ω-phase increased as it was found by X-ray technique.

The TEM analysis showed that high pressure treatment results in the change of the ω morphology together with the additional growth of the individual ω - particles. In fig. 13b the dark field electron micrograph shows the ω particles in α'plate after pressurizing the specimen. Thin plates of the ω particles, which were observed before pressurizing (fig.13a) were found to have grown after high pressure treatment. The ω particles also became more rounded and elliptical in shape (fig.13b) in comparison with their original plate form.

Ti 14% V alloy

Fig. 14a shows the morphology of as-quenched Ti-14% V alloy. Very fine α' needles in the β-matrix (marked by arrows) appear in the bright field. The inset in fig.14a shows the dark field image of the ω particles in as-quenched specimen.

Fig. 14b represents the morphology of the sample which was subjected to 9.2 GPa pressure; two effects, which follow as a result of high pressure treatment, can be pointed out:

a) The growth of α' needles (see α' needles in fig.14 a marked by arrows and compare them to α' martensitic plates in fig.14b).

b) The growth of ω particles (see inset in fig.14b which represents the dark field image of the ω particles after pressurizing the specimen.

The magnification for inset 14a and 14 b is the same).

An increase in the amount of the ω phase in pressurized specimen was also detected by X-ray analysis (Table II).

Ti 18% V and Ti-20% V alloy

The retained β phase and the ω phase were observed in the as-quenched specimens. The formation of α' phase was suppressed. Dark field TEM micrograph taken from the ω-reflection shows the elongated ellipsoidal shape of ω particles (see inset "a" in fig.(15).

The high pressure treatment at P=7.5 GPa increases the amount of the ω phase and also effects its morphology. The ellipsoidal shape of the as-quenched ω is changed and tends to be cuboidal after pressurizing. Inset "b" in fig.15 represents the dark field image of pressurized specimen. Some of the ω particles which have approximately cuboidal shape are marked by arrows. High pressure treatment also results in the appearance of α' martensite which is induced in the β metastable matrix. Bright field image of the pressure induced α' martensitic plates is presented in fig.15. Habit plane of pressure induced α' martensite was found to be ~(334) type (actually {9,7,14}) which is compatible with the results of Wood [25] for the habit plane {9,7,12} for deformation induced α' martensite in Ti-Mo alloy.

Ti-30 and Ti-35% V

Figs. 16a and 16b show a selected area diffraction pattern with zone axis $[310]_\beta$ obtained from a Ti-30% V quenched alloy and a Ti-30% V pressurized alloy respectively. In fig.16a the diffuse scattering is faint whilst fig.16b exhibits intensive diffuse streaking which could be ascribed to a ω-like formation caused by high-pressure treatment. (Similar diffuse intensity patterns for as-quenched Ti and Zr-based alloys were observed by Williams et al [48] and by Sass [49].

X-ray Analysis

Fig 17 shows the X-ray diffractograms of some as-quenched alloys and alloys that were initially quenched and then pressurized. The results of phase content analysis and lattice parameters determination are summarized in Table II. Fig.3b shows the variation of molar volumes for alpha, beta and omega as a function of composition. The data of X-ray analysis are in accordance with TEM observation for Ti with 6-20% V alloys and indicate that the ω phase remains in substantial quantity after high pressure release. In our experiments pressure was not so high as to cause 100% omega transition. Besides, the reverse transformation to the parent phase could partially take place during the pressure release. Thus the maximum amount of ω of about $\approx$ 57 vol.% was obtained (for Ti-14% V alloy).

From the data presented in Table II, it follows that the specific volume V^{α} for α phase depends on vanadium content more than the specific volume V^{β} does for β-phase (see fig.3). The axial ratio $C_o^{\omega}/a_o^{\omega}$ for the ω phase increases with the increase of vanadium content but does not remain constant as it was reported in [37]. (It should be pointed out that our results were obtained for the case when the ω phase was formed by high pressure diffusionless treatment. Thus, the composition of the ω phase depends only on composition of the original alloy and is not influenced by the diffusion process).

The increase of $C_o^{\omega}/a_o^{\omega}$ with the increased vanadium content can indicate the weakening of atomic bonds in the ω phase when vanadium concentration in the ω phase increases. This result is an indirect evidence of the decrease of those parameters which characterize the ω lattice strength such as Debye temperature, Young modulus etc., with the increase of vanadium content.

Another important result is that specific volume increment $\Delta V^{\beta\to\alpha}$ is negative ($\Delta V^{\beta\to\alpha} < 0$) when vanadium content is more than 15%. Therefore high pressure will provide driving force $\Delta V \cdot \Delta P$ for both $\beta\to\alpha$ and $\beta\to\omega$ transformations ($\Delta V^{\beta\to\omega} < 0$ for all concentration range).

3.3. Discussion

3.3.1 The sequence of diffusionless transformation in Ti-Mo and Ti-V alloys.

The experimental results can be readily explained when we consider the calculated diagrams T-X and P-X (see figs. 1,4,5,6). When the alloy content is 0-3% Mo or 0.8% V the lines of the free energy equilibrium $T_0^{\beta\to\alpha}$ and $T_0^{\beta\to\omega}$ on T-X diagrams are far from each other. Therefore, during quenching from β region the alloy first undergoes transformation $\beta\to\alpha'$ at the temperature greater than $T_0^{\beta\to\omega}$. The β phase is completely transformed to α' phase before the line $T_0^{\beta\to\omega}$ is reached during cooling. Thus only the α' phase is observed in 0-3% Mo or 0-8% V regions upon quenching.

Applying high pressure at 300°K to the as-quenched structure (α' martensite) induces the $\alpha'\to\omega$ transformation and after the pressure release $\alpha'+\omega$ mixture persists by virtue of $\alpha'\to\omega$ transformation hysteresis. During our experiments we could not observe in situ how far the process $\alpha'\to\omega$ develops and neither could we estimate which fraction of the high pressure induced ω remains at P=1 atm.

The sequence of transformations in metastable Ti-0-3% Mo or Ti-0-8% V alloy is as follows:

$$\beta \xrightarrow{\text{Quench}} \alpha'(\beta) \xrightarrow{\text{Pressure}} \alpha'(\beta)+\omega(\alpha')$$

The symbols in brackets indicate phases from which the obtained structures originate.

In the alloys with ∿ 4-10% Mo and 8-14% V the curves $T_0^{\beta\rightleftarrows\alpha}$, $T_0^{\beta\rightleftarrows\omega}$ and $T_0^{\alpha\rightleftarrows\omega}$ (and the corresponding martensite start temperature lines $M_S^{i\to j}$) are in near vicinity from one another. (The small distance between $T_0^{i\to j}$ and $M_S^{i\to j}$ lines is the consequence of a moderate value of the activation energy for $\beta\to\alpha'$ and $\alpha'\to\omega$ transformation in Ti-V and Ti-Mo systems. Therefore for 4-10% Mo (8-14% V) concentrations, the quenched β phase is not transformed to α' phase alone, since the $\alpha'\to\omega$ and $\beta\to\omega$ transformations are also expected to occur. Thus the as-quenched structure consists of β matrix with ω particles and α' needles which contain fine and regularly arranged ω plates. It is not clear as yet whether the ω plates observed in α' needles in Ti-V alloy (see fig.13a) are α'-originated. We need further experimental research to answer this question.

When high pressure is applied, the α' and ω phase grow at the expense of β phase. In Ti-V alloys the ω phase morphology changes after pressurizing and ω particles become more rounded.

The diffusionless reactions for 4-10% Mo (8-14% V) concentration range can be described as follows:

$$\beta \xrightarrow{\text{Quench}} \alpha'(\beta)+\overset{?}{\omega(\alpha')}+\omega(\beta)+\beta_{\text{retained}} \xrightarrow{\text{Pressure}} \beta+\alpha'(\beta)+\overset{?}{\omega(\alpha')}+\omega(\beta)$$

As it follows from calculations of free energy changes for these transformations (Sec 2) the pressure of about 20-30 GPa is necessary in order to complete β→α' and/or β→ω transformation in this concentration range. Besides, the higher the molybdenum (vanadium) content the greater must be the pressure $P_0^{\beta\to\omega}$ and $P_0^{\beta\to\alpha}$ (see Fig.4,6). On the other hand the phase hysteresis does not considerably depend on the value P_0 [illegible]. Therefore, it should be expected that upon releasing the pressure reverse transformation in alloys with higher vanadium content will start at higher pressures. Consequently, a smaller amount of the pressure induced phase will remain after unloading. It was this fact that was experimentally observed.

For alloys with molybdenum content less than 15% (V < 25%) but more than 11% β→ω transformation is observed upon quenching. It is in agreement with the diagrams in Fig.1,5, where only $T_0^{\beta\to\omega}$ curve will be crossed during cooling from β state. The formation of the ω-phase will be enhanced by high pressure as follows from (P-X) part of Fig. 4,6. The sequence of diffusionless transformations can be described as follows:

$$\beta \xrightarrow{\text{Quench}} \beta + \omega(\beta) \xrightarrow{\text{Pressure}} \beta + \omega(\beta)$$

When the molybdenum content is more than 15% (25% for V) the β phase is well stabilized and it remains after quenching. As it follows from Figs. 4,6 pressure that is high enough can promote β→ω transformation. According to J. Williams et al. [48,31] the β→ω transformation proceeds as an ordering process of linear displacive defects in <111>$_\beta$ atomic rows. Initially the short range correlated displacements appear and result in the characteristic diffuse streaking. When driving forces for β→ω phase transformation increase further due to cooling or to the increase of pressure, the long range correlated displacements appear, the final ω phase is created and the diffuse effects get transformed into well-resolved ω diffraction patterns. This was shown during cooling for Ti-Fe and Ti-Mo alloys in [39]. After high pressure application this effect is observed by us in alloy Ti-15 Mo. (In more detail the diffuse scattering will be discussed in Sec.5.3.2).

3.3.2 On changes in ω phase morphology in Ti-V alloys after high pressure application

As we have already pointed out the high pressure treatment of the Ti-V alloys substantially influences the morphology of the ω phase. In all investigated alloys the ω particles become more rounded after applying high pressure. The images of the ω particles in our electron micrographs are not sharp, and it may be considered as an evidence of coherency strains associated with the ω/matrix interface [52]. This implies that the ω phase morphology may be determined by minimisation of the total of the surface and strain energy. Williams and Blackburn [54, 55, 36] have suggested that the ω particle morphology can be related to the misfit between the particle and matrix lattice. In those systems where the misfit is high (> 1.0 pct) (Ti-V, Ti Fe, Ti-Cr) the particle shape is determined by the minimisation of the elastic strains in the matrix. In low misfit systems (Ti-Mo, Ti-Nb) the particle shape is governed by the minimisation of the surface energy. In the present study the changes in the ω morphology cannot be associated with the misfit changes. The compressional changes of the lattice parameters and volumes of both the ω phase and Ti-matrix are approximately the same, therefore the changes in misfit values due to the lattice parameter shift produced by pressurizing are practically negligibe. Besides, the pressure induced growth of the ω particles is not accompanied by composition changes. Thus in high pressure experiments the misfit cannot be influenced by the composition variation. On the other hand, we may assume that the surface energy term associated with the coherent ω/matrix interface is rather small in comparison with the strain energy term. Since the degree of coherency is not changed after high pressure application, the strain energy term remains predominant.

The only reasonable cause which influences the elastic energy of the ω particles in our compression studies is the change in the rigidity of the matrix. The rigidity of the matrix increases after applying high pressure. Thus the strain energy associated with the ω/matrix interface will increase. It follows that the particle which grows during pressurizing will tend to reduce its interface area. Thus more rounded shapes of the ω particle will be favourable after pressurizing.

3.3.3. Diffuse scattering effects

At the present moment the diffuse scattering effect is ascribed to a short range order displacement of short atomic rows [45,56,55]. As a result of such a displacement a short range ordered state [45] or zone is created. These zones serve as the places where ω phase eventually arises in its final shape when the change from short to long-range ordered displacement takes place under an increasing driving force. In the same sequence the diffuse streaking is changed to sharp ω reflections

The following picture can be seen by summarizing the above experimental data:

a) Diffuse scattering was not observed for alloys containing α'-phase in the as-quenched state (3 to 5 at.% Mo).

b) Diffuse scattering occurs in as-quenched β phase alloys with higher Mo concentration (11 to 18 at.%). An intense diffuse network was observed in the Ti-15% Mo alloy (fig.10b), bordering on the region where ω is still observed (fig.1).

c) After hps of the Ti alloys with 18 to 25% Mo a weak diffuse scattering is observed together with secondary ω-like reflections.

Since the appearance of diffuse scattering relates with concentration we may use the results of the phase diagram calculation. The calculation predicts that at 300K the alloy with 15% Mo has to be out of all the alloys under study, nearest to the $\beta \to \omega$ phase equilibria line. Consequently, this alloy in the as-quenched state must display maximum instability of the β-matrix. In alloys with less Mo the instability of the β phase "discharges" in the advent of the ω phase in the course of fast cooling during quenching. Therefore these alloys might have minimal or not at all diffuse scattering.

In alloys with Mo > 15% one has to observe diffuse scattering decreasing with the **the** amount of Mo.

The application of high pressure to these alloys instantaneously increases the amount of ω phase due to an increase in the driving force for $\beta \to \omega$ transformation. Simultaneously, instability of regions of β matrix not yet transformed, grows, giving rise to an ordered displacement of atomic rows and appearance of diffuse scattering as a precursor of its complete transition to the equilibrium form of the ω phase.

In the case of Ti with V > 30% V according to the calculations the $\beta \to \omega$ transformation should be expected to start at fairly high critical pressure. Well resolved ω diffraction pattern should be expected; however, destruction of the ω phase begins during unloading, and only short-range correlated displacements remain at 1 atm. giving rise to very intensive diffuse streaking. The diffuse streaking for pressurized specimen is more intensive than that for the specimen in an as-quenched condition. Thus we can conclude that in addition to 111_β displacements caused by quenching the high pressure treatment results in appearance of new short range correlated displacements in the lattice. These displacements are certainly static in nature because they are due to the pressurizing and cannot be related to changes in temperature.

3.3.4. The correlation between the phase stability and basic physical properties of the Ti-V and Ti-Mo alloys

Comparison of experimental and calculated phase diagrams, in the Ti-V and Ti-Mo systems disclose the same features in phase stability and succession of phases due to alloying and application of high pressure. Pressure induces these changes more efficiently in the Ti-Mo system. This seems natural since both elements have atomic radii which are smaller (r_V=1.34) and r_{Mo}=1.39 Å) than that of Ti (r_{Ti}= 1.47 Å) while both of their valency electron concentrations are larger. Alloying Ti with V and Mo could be considered as analogous to applying high pressure, since both diminish the mean atomic volume and increase the valence electron concentration, $\dot{n}_e$. This point of view has been presented many times (recently in [57] in an attempt to explain phase transformations as stemming from changes in electron-to-atomic ratio or d-band occupancy (ΔN_d^c)[57], electronegativity, etc. These physical models are qualitative since they cannot take into account changes in lattice vibration parameters and electron-phonon interaction caused by changes in composition and pressure. Thus, it is impossible to change ΔN_d of transition metal by alloying by an amount which is equivalent to that induced by pressurization without altering the average weight of the atoms in the lattice and, as a consequence, substantially change lattice properties and electron-phonon interactions. In the present case one has to add twice as much V to titanium than Mo to obtain the same increase in the number of d-electrons. However due to the great difference in atomic weights (V=50.94, Mo=95.94) this immediately creates a strong difference in Ti-V and Ti-Mo lattice dynamics. For these reasons it is difficult to predict quantitatively the behavior of transition metals alloys from first principles, while the thermodynamic approach can be applied successfully. On the other hand, establishment of correlations between phase stability and basic physical properties (Debye temperature θ_D, electronic specific heat coefficient γ_{el}, critical superconducting temperature, T_c, etc.) can help rationalize the source of phase stability under some conditions.

A complete set of physical data for Ti-Mo [58] and Ti-V [59] systems obtained by Collings et al. is now available as shown in Figure 8. It is instructive to examine the trends observed when Ti is alloyed with Mo or V and compare the results with pressurization of these alloys in a metastable state.

1. In the phase diagram regions with 0-4% Mo or 0-8% V, α' is stabilized upon quenching and the ω phase arises under pressurization. As the Mo/V concentration increases the $P_S^{\alpha' \to \omega}$ decreases. The α'-phase is the most stable phase at [illegible] since α' has larger vibrational entropy relative to ω (i.e. $\theta_D^{\omega} > \theta_D^{\alpha'}$) in spite of the destabilizing influence of α' phase's higher electron density*, $E_{el}^{\alpha'} > E_{el}^{\omega}$ since $\gamma_{el}^{\alpha'} > \gamma_{el}^{\omega}$. The b.c.c. β phase is unstable in pure Ti at room temperature since its θ_D^{β} is much less than $\theta_D^{\alpha'}$ and $E_{el}^{\beta} > E_{el}^{\alpha'}$. The addition of Mo or V decreases $\theta_D^{\alpha',\omega}$ and increases $n(E_F)$ but at different rates. The application of pressure to any particular alloy of fixed concentration [illegible] increases θ_D and $n(E_F)$ (i.e. E_{el}) in both phases. The α' phase destabilization and ω phase appearance may be attributed to a more drastic increase in $n(E_F)^{\alpha'}$, which can be inferred from T_c behavior under pressure (Figure 8) [illegible] an increase of $E_{el}^{\alpha'}$ and a decrease of the thermodynamic "barrier", $\Delta F^{\alpha' \to \omega}$, for ω phase formation which must be "overcome" by the [illegible]. As [illegible] decreases, $P_S^{\alpha' \to \omega}$ decreases.

2. In the intermediate regions with [illegible] Mo [illegible] 15 [illegible] 10 [illegible] V, two or all three phases are found to coexist upon quenching. Under pressure, the β phase disappears while the amount of ω [illegible] increases. In this range the

---

* It is considered that the vibrational entropy of a particular phase, S_{vib}, is smaller, as its θ_D, the vibrational characteristic temperature, is higher [60]. The internal energy (E_{el}) component is proportional to $n(E_F)$ [illegible] [60] where $n(E_F)$ is density of states at the Fermi level.

concentration of Mo/V is still insufficient to stabilize the β phase completely. The following relationships are observed:

$n(E_F)^{\omega} > n(E_F)^{\alpha'}$ [illegible] $n(E_F)^{\beta}$, [illegible] $\theta_D^{\alpha'}$ [illegible] θ_D^{β} , i.e.

E^{ω}_{el} [illegible] $E^{\alpha'}_{el}$ [illegible] E^{β}_{el} S^{ω}_{Vi} [illegible] S^{β}_{Vi} ; S^{ω}_{Vi} [illegible] $S^{\alpha'}_{Vi}$, where

S^{i}_{Vi} is the vibrational entropy component. The configuration component of the entropy, S_{con}, is the same for all three phases in question for a diffusionless transformation. As Mo/V concentration increases, S_{Vi} and E_{el} decrease since θ_D increases and $n(E_F)$ decreases. The marked increase of θ_D in Ti-Mo is a result of alloying, and clearly demonstrates the influence of atomic weight of elemental components in an alloy. The ω and α' phases exhibit different behavior. Their $S^{\alpha'}_{Vi}$ and $E^{\alpha'}_{el}$ increase with Mo/V addition. Under pressure, destabilization of β relative to α' occurs due to the rapid increase in E^{β}_{el}. The latter stems from an increase in lattice specific heat contribution because θ_D increases under pressure causing a decrease of S_{Vi}. A similar situation prevails for [illegible] phase equilibria where the disappearance of [illegible] phase is due to an increase in the electronic contribution to its energy.

The sharp increase in the critical pressure of [illegible] transitions under pressure at 300K, $P^{\beta\to\omega}_{n}$, with increase of Mo/V content [illegible] small values of [illegible]. Figure 3 shows that there are small [illegible] in alloys where α' can be induced by pressure at the expense of the [illegible] phase in titanium alloys with more than 5% molybdenum or titanium [illegible] with more than 15% vanadium.

When the Mo concentration exceeds 15% and the vanadium concentration exceeds 25% the β phase is retained upon quenching. Here the [illegible] phase is formed under pressure at 300K with a higher $P^{\beta\to\omega}_{S}$ at larger Mo/V concentration. The physical relationships that follow $(n(E_F)$ [illegible] $n(E_F)$ [illegible], θ_D [illegible] θ_D) from Fig. 6 suggest that

S_{Vi}^{ω} must be less than S_{Vi}^{β}. From a phenomenological point of view this situation is quite understandable: there is an energetic barrier to the [illegible] transition which the Mo/V concentration increases. Since $\Delta V^{\beta \to \omega} < 0$ in all concentration ranges, larger pressures are required to overcome this barrier as the alloy content increases. Nevertheless the relationships between physical properties of β and ω phases in these concentration ranges differ from that in intermediate ranges. Consequently pressure application should increase the β phase stability relative to ω, since pressure increases θ_D^{β}, decreases θ_D^{ω}, decreases $n(E_F)^{\beta}$ and probably increases $n(E_F)^{\omega}$, according to Fig. 18. The question then arises as to how the transformation occurs under pressure. [illegible] it is likely that some additional peak in $n(E_F)^{\omega}$ concentration/pressure dependencies might exist which are not revealed in [50]. This is probable in the Ti-Mo system where:

a) Spinodal decomposition observed with a miscibility gap located at ~25% Mo, instead of being located at [illegible]. Therefore, some additional peak in [illegible] function may be created by configurational contribution to entropy and peculiarities in the internal energy as a function of pressure or concentration. b) The increase of superconducting temperature T_c with pressure observed for alloys with Mo ~15% [50], also indicates that the ω phase has some peculiarities in its electron structure.

The final possibility is that the present estimate of θ_D and $n(E_F)^{\omega}$ for these alloys is wrong and that $n(E_F)^{\omega}$ [illegible] $n(E_F)^{\beta}$ and θ_D^{ω} [illegible] phase is denser than β. If this were the case, application of pressure would stabilize ω relative to β as a result of lattice vibrational contributions. Here again some energetically expensive peculiarities in the electronic spectrum of the β phase which control $n(E_F)^{\beta}$ and F_{el}^{β} under pressure could favor the appearance of ω phase. This qualitative discussion displays some of the difficulties in developing an explicit picture of the influence of alloying and compression on the sequence in phase stability in Ti-Mo-V alloys. Nevertheless, the present thermodynamic analysis provides a method of predicting the correct sequence of phase stability with concentration, temperature and pressure.

3.3.5 Mechanical Properties of Ti-Mo alloys

In [61] the mechanical properties of Ti-11 wt.% Mo (~5 at.%) was reported and in [62] the mechanical properties of several Ti-Mo alloys (up to 25 wt.% Mo. or up to 11 at.% Mo) were investigated. [62] deals with the effect of thermal history and the obtained microstructure on σ-ε curves of β-quenched Ti-Mo alloys. Low yield stress, σ_y, was obtained for as-quenched samples for pure Ti, ~3.5, ~5 and ~7 at.% Mo. Low σ_y for quenched 3.5 - 7 at.% Mo was explained by the possibility of strain induced transformation of retained β phase, β→α'. Mechanical properties of Ti - 7.2 at.% Mo were investigated in [63]. Embrittlement was found in the quenched samples after ageing at 350 C for 15 hours and was explained by the interaction of dislocation pile-ups with relatively large ω-phase particles formed during ageing. In [65] plastic deformation and thermally activated dislocating kinetics were investigated in Ti-6.5 at.% Mo (α+β) and Ti - 15.2 at.% Mo β alloys. The results were explained in the frames of thermally activated overcoming of oxygen interstitials by moving dislocations. The effect of composition and heat treatments on mechanical properties of various Ti alloys including Ti-Mo alloys was studied in [12,41,64]. It was shown that a dislocation may bypass the ω-phase particles and if the amount of ω-phase < 25 at.% [illegible] ω-phase has very little effect on the strength and ductility. In [65] the deformation behavior of Ti-Mo alloys with α, β and ω-phases was investigated and from the TEM data it was [illegible] that the density of ω-particles decreases within the slip bands and that in α+β alloys α phase serves as a crack arrester. In [66] the thermally activated deformation of precipitation hardened [illegible]-Ti (40V [illegible]) [illegible] single crystals is reported and [67] reports the effects of a second phase dispersoids on the deformation behavior of Ti. The influence of various heat treatments on microstructure, σ-ε curves and fracture toughness in a metastable β-Ti-1[illegible] at.% Mo was studied in [68]. It was found that precipitation occurs on ω particles resulting in a very fine distribution of the α phase with increased strength and good fracture toughness accompanied by limited ductility.

This research studied the influence of composition and phase composition, obtained as a result of high pressure treatment and of heat treatment of previously quenched samples on the mechanical properties of Ti-Mo alloys. The tests were conducted in compression on an Instron testing machine (model 1195). The yield stress, σ_y, was defined by a deflection of [illegible] from the elastic line. The dimensions of the samples used in the experiments were 5 mm length, 2.5 mm dia., providing high pressure treatment up to 9.0 GPa in the existing pressure cell, described in 3.1. The cross head speeds used were $S = 5 \mu m/min$ and $S = 50 \mu m/min$ providing strain rates of $\dot{\varepsilon} = 10^{-5}/s$ and $10^{-4}/s$ correspondingly.

In Fig.18 the yield stress, σ_y, obtained at $\dot{\varepsilon} = 10^{-5}/s$ is shown in dependence on composition for Ti-Mo alloys after various treatments: as-quenched, quenched + high pressure treatment, 9.0 GPa, 2 hours and quenched + annealed for 2 hours at 350-380°C. All these treatments were used also for microstructure investigation using TEM and X-ray analysis as reported in previous sections. As it may be seen from Fig.18 the lowest σ_y in as quenched samples is observed for Ti-8Mo alloy. And for the same alloy the highest σ_y is observed after high pressure treatment and after annealing. Fig.19 presents the stress-strain curves for Ti-8Mo alloys after various treatments. It may be seen that for as quenched samples the strain hardening is also appreciably lower than for high pressure or heat treated samples. σ_y obtained at $\dot{\varepsilon} = 10^{-4}/s$ was by 2.8% higher than that obtained at $\dot{\varepsilon} = 10^{-5}/s$. For all compositions after various treatments quite high plastic deformation, exceeding 15% was obtained, the main limitation being elastic instability of plastically deformed samples. According to the result of X-ray and electron microscope analysis of phase content, presented in Table 1, alloys with an amount of

Mo $\geq$ 15% are stable β alloys with some additions of ω phase after high pressure soaking or after ageing. It can be seen from Fig. 19 that these additions don't effect σ_y in alloys with content of Mo $\geq$ 18%. Table 1 doesn't present the data of phase content for Ti-6% Mo. According to the analysis for Ti-8% Mo as quenched samples contain 80% of β phase and 20% of ω phase, high pressure treated samples contain 55% of β phase, 32% of ω phase and ~ 13% of α phase, after ageing the samples contain 51% of β phase, 49% of ω phase and traces of α phase. It seems that there is only a quantitive difference between as quenched and aged samples the ratio of ω/β being higher for aged samples. At the same time σ_y of aged samples is 3.5 times higher than that of as quenched samples. The difference in phase content is negligible if we will compare as quenched samples of Ti - 8% Mo alloy with samples of Ti - 11.5% Mo after high pressure soaking (see Table 1) but the σ_y of the last ones is almost twice as high as that of the first ones. The difference was found in the dimensions of ω phase particles, that were observed as large disks with 150-600 Å dia in aged samples, 50 - 300 Å dia for high pressure treated samples and very small precipitates in as quenched samples.

It may be expected that the instability of ω or β phases or both of them is a reason for a very low σ_y and low strain hardening of as quenched samples of Ti-8 Mo alloys. Such instabilities may cause $\beta \to \omega$ and $\beta \to \alpha$ phase transformations at relatively low shear stresses. In order to check one of the possibilities the as quenched samples of Ti-8 Mo alloy were deformed plastically to ε = 5% and an X-ray analysis of phase content was conducted. From this analysis follows that there is an increase of α phase content from traces to ~ 12% as a result of $\beta \to \alpha$ phase transformation. In high pressure treated and aged samples relatively large precipitates of ω phase work apparently as barriers for α phase growth. If the nucleation of α phase starts on ω particles as in [68] the conditions for such nucleation may not be the same for very small precipitates in as quenched samples and for relatively large particles of ω phase in pressure and heat treated samples. Additional information on dislocation mobility and on barriers for dislocation motion may be obtained from thermally activation analysis of plastic deformation. That may provide data on entalpy of activation and the area alloys after various heat treatments. Using new methods, stress jump and temperature jump during plastic deformation the influence of changes of dislocation structure may be eliminated [69]. Preliminary results on activation area Δa obtained in Ti-8Mo alloys using stress jump method show that in as quenched samples Δa is appreciably higher than that obtained in high pressure treated or aged samples. Detailed thermal activation analysis using temperature jumps and barrier profile analysis [69] may provide data for more comprehensive discussion of dislocation mobility and mechanisms of plastic deformation in various Ti-Mo alloys with different phase content and phase morphology.

It may be noted that from the point of view of the influence of ageing 350 °C on mechanical properties in Ti-8Mo alloy one hour of ageing gives almost the same σ_y as ageing for 72 hours, used for [illegible] investigation. More than 80% of this σ_y (after 72 hours ageing) is obtained after 15 min of ageing at the same temperature. It is of interest to investigate the changes in phase content and phase morphology after such treatment

4 Conclusions

1) The metastable T-C and T-P phase diagrams of Ti-Mo and Ti-V alloys were calculated using Kaufman's regular solution approach and the experimental data obtained in the present work. The calculated phase diagrams are in satisfactory agreement with the structural data obtained. These give also useful directory for predition of phases appearance/disappearance under changing temperature and pressure conditions

2) In metastable Ti-Mo and Ti-V alloys considerable amounts of the ω phase can be formed at elevated pressures and remain at atmospheric pressure. The [illegible] and $\beta\to\alpha'$ high pressure transitions were observed first in Ti-based alloys. The new crystal structures, which have not been obtained after conventional treatment, were produced by high pressure application at 300K. The substantial changes in ω phase morphology occur in Ti-V alloys being subjected to high pressure.

3) The effect of high pressure was compared with the influence of alloy contentration on metastable diffusionless equilibria in Ti-Mo and Ti-V systems. As the content of Mo/V increases, the pressurizing and alloying effects start acting in opposite directions; pressurizing, in contrast to alloying, reduces the β stability and stimulates the $\beta\to\alpha'$ and $\beta\to\omega$ transformation.

Acknowledgements

The authors wish to express their deep gratitude to Dr. [illegible] Davidson, Dr [illegible] Kendall, C. Homan and J. Frenkel of Bennet Weapon Lab. at Watervliet Arsenal for their encouragement, support and warm hospitality during the project.

To Dr, R. Weiss, who helped us to establish personal contacts with the European Office of the USA Army; and to Dr. R. Quattrone of the Army Research Office in Europe for his support and warm reception in London

Appendix 1

THE STRUCTURAL STABILITY AND SUPERCONDUCTIVITY OF Ti-Mo ALLOYS UNDER PRESSURE*

The influence of hydrostatic pressure on the transition temperature to superconductivity T_c was studied on Ti-Mo alloys with 3-35 at% Mo up to about 9.5 GPa. The pressure effect on T_c is positive, i.e. T_c increases under pressure. The effect becomes smaller with increasing Mo concentration and vanishes for $Ti_{65}Mo_{35}$. The results can be understood by the increasing instability of the metastable alloys under pressure.

I Introduction

In the past the high pressure behaviour of T_c, the transition temperature to superconductivity, has been studied for several transition metal alloys. All the investigated alloys (Ti-V, V-Cr, Zr-Nb, Nb-Mo, Hf-Ta, Ta-W)[72,73,74] were continuous solid solutions between neighbouring elements in the bcc-structure (β-phase structure).

Considering the change of T_c due to alloying or to applying high pressure, a correlation was found between changes in T_c and changes of the electron density of states at the Fermi-level $n(E_F)$. For these systems application of pressure was always at least qualitatively equivalent to adding electrons to the conduction band by alloying. Using this correlation it was possible to predict the sign of the pressure effect dT_c/dp knowing the data for $n(E_F)$ and T_c as functions of the valence electron number n_v in each particular system. In all alloys mentioned above the pressure effect is positive ($dT_c/dp > 0$) if the density of states $n(E_F)$ increases with increasing n_v and vice versa.

---

* This part was done in Physical Institute of the University Karlsruhe, W. Germany. A. Rabinkin took participance in this part together with H. Scherev, D. Köhnlein and W. Buckel. The samples studied in Se were used.

In this paper the high pressure experiments are extended to Ti-Mo alloys. Ti and Mo are not neighboring and not even situated in the same row of the Periodic Table. This system was chosen since a series of careful studies on Ti-Mo alloys already exists [75,76] and since the samples used for the pressure experiments have been extensively characterized with regard to their structure in Sec. 3.

Ti and Mo have very different atomic radii (r_{Ti} 3+ = 0.76 A; r_{Mo} 6+ = 0.62 A) r_{Mo} 6+ = 0.62 A). Therefore in a rough approximation, one could expect that alloying Mo acts as pressure, i.e. decreasing the lattice constant. Also the valence electron number n_v is increased by adding Mo to Ti. As a result of the earlier experiments we know that increasing n_v also corresponds to the application of pressure. Since the electron density of states $n(E_F)$ for the bcc alloys structure of Ti-Mo has been found by Ho and Collings [75] to decrease monotonically with increasing Mo-content a negative pressure effect ($dT_c/dp < 0$) could be expected from the earlier experiments for alloys with Mo ≥ 16%.

It was the aim of the present work to measure the T_c(p)-dependence of Ti-Mo-alloys and to check whether the correlation found for alloys of neighboring transition elements also holds for such a more complex system. This is apparently not the case.

II. Samples and their structure

The details of sample preparation and the description of their structure in the as quenched state and after pressure treatment is discussed in Sec 3.

Here only a few results should be quite briefly mentioned. At sufficiently high temperatures all Ti-Mo-alloys are single phase bcc(β-phase). On quenching alloys from the β-field to room temperature a sequence of non-equilibrium structures appears. From a structural point of view, all samples should be classified into three groups:

a) 0-4.5 at% Mo: Two martensitic phases α' and α'' exist.

b) 5-15 at% Mo: The sample consists of a mixture of β-phase stabilized by the quenching and rather finely dispersed ω-phase.

c) ≥ 18 at% Mo: Only the β-phase can be detected.

Generally, high pressure favours the formation of the ω-phase.

With regard to superconductivity, the concentration dependences of $n(E_F)$ and θ_D determined by Collings et al. [76] are essential (see Sec.2, fig 18). For the β-phase a monotonic decrease of $n(E_F)$ has been found. In the concentration range c_{Mo} < 18 at% Mo, where only the β-phase exists in a mixture with the ω-phase, the density of states $n(E_F)$ has been calculated for a "virtual" β-phase.

The transition temperatures measured by Ho and Collings are given in fig. 21. For the α'' and α' region a steep increase of T_c with increasing Mo-content has been observed. This enhancement of T_c is attributed to extreme lattice distortion resulting from the occurrence of the α''-phase and increasing the electron-phonon coupling.

The distinct maximum of T_c for c_{Mo} ≈ 5 % has been explained by the occurrence of ω-phase. For Mo-concentration below about 10 % increasing [illegible] finely dispersed ω-phase [illegible] exist in the β + ω mixture [illegible] decreasing T_c of the β phase [illegible] otherwise [illegible] increasing Mo content [75].

[illegible] Experimental details

The T_c-measurements at high pressure were carried out in an equipment described earlier [77,78]. Solid-state cells with steatite as pressure transmitting medium were used. A Pb-strip as an internal manometer was always placed into the pressure cell together with the alloy sample. The pressure inside the cell was determined using the $T_c(p)$-dependence of Pb as calibrated by Eichler and Wittig [79]*.

---

* This calibration has to be shifted to somewhat lower pressures [illegible]. However this correction is not essential for the results reported here.

Of course, some pressure variation from the center to the periphery of the cell always exists within solid state cells. However, since the transition curves under pressure have almost the same sharpness as those at normal pressure (see fig. 22a) one may conclude that this pressure variation does not very much influence the result.

The electrical resistances of the alloys sample and the Pb-manometer were measured by the four probe method. It has to be mentioned that this technique is especially sensitive to areas with high T_c since a single superconducting path can short-circuit the whole sample.

A calibrated Allen-Bradley carbon resistor was used for measuring the temperature.

All step-by-step loadings of samples were done only at room temperature. This was necessary since one knows from earlier experiments that lattice defects can strongly influence T_c when they are induced by deformations at low temperatures. However, these defects disappear almost completely by annealing processes at room temperature [80].

IV. Results and discussion

Fig. 21 gives the transition temperatures of our samples measured at normal pressure (x). T_c is defined as the value for $R(T)/R_n = 0.5$ (R_n = residual resistance). For comparison, the T_c-values of Ho and Collings [75] are also plotted versus the Mo-concentration. For $c_{Mo} \geq 7\%$ all samples exhibit somewhat higher T_c-values than those of [75] determined in calorimeter. This can be easily explained by the fact that resistance measurements with a four probe technique over-estimates the high T_c areas within the sample. A rather low T_c has been observed for the Ti + 3% Mo sample. However, in this concentration range T_c strongly depends on the crystal structure and especially on the volume fractions of α' and α''.

Therefore, somewhat different quenching conditions could be responsible for the lower T_c of our Ti + 3% sample. The transition curve of this sample exhibits a distinct step. A small part of the sample already becomes superconducting at 1.9 K (marked by the bar in fig. 21).

In fig. 22a the normalized resistance $R(T)/R_n$ of a Ti + 11.5% Mo-sample at different pressures is plotted versus the temperature. The transition temperature is increased by pressure. With the exception of the transition at 1.4 GPa* the width of the transition curves is not very much changed by pressure proving the sufficient homogeneity of the pressure within the cell. Fig. 22b shows the transition temperature of this sample as a function of pressure. The increase of T_c with pressure is almost linear within the used pressure range. This linearity was observed for all samples.

In fig. 23 the pressure effect $d\ln T_c/dp$ for the various alloys is plotted versus the Mo-concentration. Also the valence electron to atom ratio is given on top of the drawing.

The pressure effect $d\ln T_c/dp$ is rather large for the 3% Mo-alloy. This alloy consists of a mixture of α'- and α''-phase.

It seems reasonable to compare this value with the pressure effect of pure Ti in the α-phase. Brandt and Ginsburg [81] reported values of $d\ln T_c/dp$ for Ti as high as $\sim 20\cdot10^{-11}$/Pa. Our value of $12\cdot10^{-11}$/Pa for Ti + 3% Mo fits satisfactorily to this result. To understand the rather high pressure effect one could argue that the formation of the ω-phase under pressure demonstrates an increasing tendency of the $\alpha' - \alpha''$-mixture to become unstable under pressure and that this increasing instability causes an enhancement of T_c.

For all other alloys we can assume that the transition temperature at normal pressure and at elevated pressures belongs to the β-phase. The pressure

---

[*] At low pressure it is somewhat questionable whether purely hydrostatic conditions could be achieved.

effect expressed by $d\ln T_c/dp$ exhibits only small variation and is positive over the whole concentration range up to 35 at.% Mo ($n_v = 4.7$). The relevant date are collected in Table 3. This result does not agree with the correlation between pressure and alloying found for alloys consisting of neighboring elements [73,74]. According to this correlation one expects a negative pressure effect for concentration ranges where $n(E_F)$ and T_c decreases with increasing valence electron number n_v. The Ti-Mo alloys apparently behave differently and show a positive pressure effect.

An obvious possible explanation of the positive pressure effect is based on the stability of β-phase. In fact, the β-phase becomes less stable under pressure. As a result the β-phase is transformed to the ω-phase which can be detected by electron microscope analysis, at least for $c_{Mo} < 35$ at.%. An increasing tendency to become unstable under high pressure enhances the electron-phonon interaction and this may also enhance T_c. This effect perhaps can outweigh the influence of the change in the electron systems. As was discussed in Sec.3.3.4 the stability of the β-phase increases with Mo concentration. Therefore the pressure effect decreases and at 35 % Mo it is almost zero. At this concentration and at pressure up to 10 GPa the alloy is far away from the critical pressure for which the $\beta \to \omega$ transformation starts (see Fig. 4 in sec. 2). It is not unlikely that an additional peak in the $n(E_F)$ curve can exist in this concentration range and can also effect on $d\ln T_c/dp$ despite the fact that according to Ho and Collings there is only monotonic decrease in $n(E_F)$. Up to now they have measured it on alloys with rather large differences in concentration.

The tendency of the lattice to become unstable at high pressure may also influence the pressure effect of the sample consisting of α'- and α''-phase. Here the stability of the α' (α'')-phases decreases under pressure. Simultaneously the steep increase in $n(E_F)$ very likely takes place as a result of a decrease in interatomic distances.

<u>TABLE 3</u>

sample	e/a	T_c (K)	$\partial T_c/\partial p$ (10^{-11} K Pa)	$\partial \ln T_c/\partial p$ (10^{-11} Pa)	Structure
Ti-3 at% Mo	4.06	1.43	1.7	11.89	$\beta' + \alpha''$
Ti-7 at% Mo	4.14	3.4	1.15	3.46	$\beta + \omega$
Ti-11.5 at% Mo	4.23	4.18	0.525	1.25	$\beta + \omega$
Ti-15 at% Mo	4.3	4.25	1.45	3.43	$\beta + \omega$
Ti-18 at% Mo	4.36	4.8	1.24	2.6	β
Ti-25 at% Mo	4.5	4.5	1.22	2.7	β
Ti-35 at% Mo	4.7	3.1	0	0	β

The pressure effect seems to pass a flat minimum at about 12 at.% Mo. Since the samples consist of ω- and β-phase in this concentration range the low pressure effect in the sample with 11.5 at.% Mo could be due to a special structure of the sample accidentally achieved. However, the quantity of ω-phase is not substantial enough to decrease T_c so strongly. Looking to fig. 4 of Sec. 2, one notices that the sample with 11.5 at.% Mo lies just between the critical pressures $P_o^{\alpha\to\omega}$ and $P_o^{\beta\to\omega}$. At present one can only point to this fact without giving any further explanation.

Appendix 2

THE α→ω POLYMORPHOUS PHASE TRANSFORMATION IN PURE Ti AT ATMOSPHERIC PRESSURE

Introduction

Since Jamieson's discovery of the ω phase in Zr subjected to high pressure [1] much work has been published specifying details of the polymorphous α→ω phase transformation. Resistivity measurements and X-ray analysis have been used as the main experimental methods.

There was a great discrepancy in data concerning values of equilibrium pressure $P_0^{\alpha\to\omega}$, and critical start pressure, $P_S^{\alpha\to\omega}$, for the α→ω transformation especially at temperatures close to 300K. The minimal values of $P_0^{\alpha\to\omega}$ (300K) = 2.2 ± 0.5 GPa and $P_S^{\alpha\to\omega}$ (300K) = 3.0 GPa were reported by Zilbershteyn et al. [6] on the basis of measurements of resistance to shear under conditions of simultaneous application of high pressure and shear stresses.

Meanwhile the correct determination of the pressure dependence of $P_0^{\alpha\to\omega}$ is of fundamental importance since it then becomes possible to calculate the value of dP_0/dT and then to obtain all basic thermodynamic parameters of the phase transformation in which the ω phase participates in Zr and Zr-based [illegible].

In our recent work [38] the appearance of the ω phase [illegible] applications of high pressure was investigated by means of [illegible]. Three different orientation [illegible] of the ω phase [illegible] were established:

$(0001)_\alpha \parallel (\bar{2}110)_\omega$; [illegible] ; [illegible]

$[\bar{2}110]_\alpha \parallel [0001]_\omega$; [illegible] ; [illegible]

These results enabled us to [illegible] complex electron diffraction patterns containing 3 variants of [illegible] presence of a small amount of the ω phase in an α matrix. Furthermore, from our experiments we found that, in comparison with electrical resistivity measurements or X-ray analysis, high resolution dark-field electron microscopy was the most sensitive method available to identify the ω phase during the very early stages of the α→ω transformation.

In the present work we constructed more accurately the region of the T-P phase diagram of Zr below room temperature and specified more exactly the pressure at which the ω phase appears at room temperature

Experimental Procedure

The foil samples ([illegible] 100 μm thickness) were prepared by cold rolling sheets of spectra-pure standardized Zr (total metal impurities [illegible]) produced by Johnson Matthey. After rolling, the foils were annealed at [illegible] K for 2 hours in a vacuum at [illegible] Pa and were then either quenched under vacuum into DC 704 diffusion pump fluid or slowly cooled. TEM specimens were then produced by electropolishing at [illegible] 210K under the conditions of [illegible] and afterwards were again annealed at 450 [illegible] in high vacuum in order to destroy any traces of the ω phase which might have been created during the electropolishing process.

Some of the annealed samples were then cooled down to [illegible], 77 and 4.2 K for 1 hour and other samples were pressurized at 300K for 2 hours at 0.5; 1.0; 2.0; 6.0 and 10 GPa.

Pressurization up to [illegible] GPa was performed in a [illegible] apparatus with a teflon cell filled by a liquid medium and it provided pure hydrostatic loading conditions. Pressurization from [illegible] to 10 GPa was performed in a solid-medium cell. Some foils in the as-quenched state were subjected to cold rolling with a thickness reduction of [illegible] and then without subsequent annealing were analyzed in the electron microscope.

3.2. Experimental Results

The characteristic electron diffraction pattern, which consists of ω phase reflections imposed on reflections of the α matrix, appears in annealed pure Zr which has either cooled down to 200K at 1 atm or pressurized at 1.0 GPa. All other samples which were subjected to higher pressures or were cooled to lower temperatures also demonstrated the presence of the ω phase. The lower the temperature or the higher the pressure the larger was the amount of ω observed [84].

The ω phase was also revealed in cold rolled specimens.

The increase in volume fraction of the ω phase with increasing driving force is associated with an increase in both the particle size and number of particles. It has to be pointed out that the characteristic ω lines on X-ray diffractograms appear only when applied pressure exceeds ~ 4.5 GPa. Besides, when pressurizing α-Zr the slope of resistivity curve changes substantially only in the vicinity of 4.0 GPa that is in agreement with data of [6,29]

3.3. Discussion

On the basis of the above mentioned results the corrected (for low temperature) T-P-equilibrium phase diagram of zirconium was constructed taking into account data from ref. [6,3,85] (fig.24). The positions of the line $T_S^{\alpha\to\omega}$, which is where the $\alpha\to\omega$ phase transformation starts, and of the line $T_S^{\omega\to\alpha}$, which is where the reverse $\omega\to\alpha$ transformation starts, were determined more correctly. On the other hand the positions of lines $T_f^{\alpha\to\omega}$ and $T_f^{\omega\to\alpha}$, where the phase transformations are completed, were more difficult to determine and some uncertainty remains concerning their precise positions. This uncertainty arises since after pressurizing at P = 10 GPa and $\alpha\to\omega$ phase transition was still not completed and the remaining α phase could be clearly observed in the electron microscope even though in this case X-ray analysis failed to detect the presence of the α phase.

The main conclusion which can be drawn from the corrected T-P phase diagrams constructed in this work is that the ω phase in pure Zr is a stable phase at ambient pressure at temperatures less than $\sim$ 200K. The corrected value of $dT_0^{\alpha\to\omega}/dp$ is equal to 116K/GPa. Since $\Delta V_{Zr}^{\alpha\to\omega} = -0.180$ cm^3/mol the entropy difference $\Delta S_{Zr}^{\alpha\to\omega} = -1.67$ J/mol·K. From the positions of the lines $T_0^{\alpha\to\omega}$ and $T_S^{\alpha\to\omega}$ and taking into account the value of $\Delta S^{\alpha\to\omega}$ it is easy now to evaluate the activation energy $\Delta F_{act}^{\alpha\to\omega}$ necessary to initiate the $\alpha\to\omega$ transformation. Thus for a temperature of 300K we obtain:

$\Delta F_{act}^{\alpha\to\omega}\Big|_{300K} = \Delta V^{\alpha\to\omega} \times (P_s^{\alpha\to\omega} - P_0^{\alpha\rightleftarrows\omega}) = 225$ J/mol and the activation energy at 1 atm. $\Delta F_{act}^{\alpha\to\omega}\Big|_{1\ atm} = 217$ J/mol

It can be seen that these values are practically equal and rather small. The small value of $\Delta F_{act}^{\alpha\to\omega}$ confirms our suggestion that the $\alpha\to\omega$ lattice reconstruction proceeds as an ordered displacement of close-packed $\langle 1\bar{2}10\rangle$ atomic rows over a short distance requiring a rather low activation energy. Such an ordering process, by analogy with the $\beta\to\omega$ transformation, might occur through two successive stages - first, creation of linear $\langle 1\bar{2}10\rangle$ defects and, then, their periodical ordering. Both stages must proceed through individual fluctuation processes which therefore would be reflected in the detailed isothermal or isobaric kinetics. Indeed, an increase in the amount of ω phase with time was observed near room temperature at constant prssure [6]. We also observed an increase in the amount of the ω phase in an α matrix when specimens were exposed at a temperature of 77K at 1 atm.

Analysis of the data of Fisher et al [27] on elastic moduli behaviour for single crystal Zr at various temperature shows that a slight positive deviation from linear dependence of moduli C_{44} takes place below 300K. On the basis of our e[illegible]al data we may suppose that the formation of the ω phase is responsible for such abnormal behaviour of the moduli C_{44}.

Analysis of the data of Fisher et al [27] on elastic moduli behaviour for single crystal Zr at various temperatures shows that a slight positive deviation from linear dependence of moduli C_{44} takes place below 300K. On the basis of our experimental data we may suppose that the formation of the ω phase is responsible for such abnormal behaviour of the moduli C_{44}.

The appearance of the ω phase in α-Zr after cold rolling can also be interpreted in terms of ω stability at room temperature. In those materials where denser phases appear under uniform high pressure, both cold rolling and compression induce the same phases. The calculations show that the driving force developed by deformation is of the same order as driving force developed by high pressure. Therefore cold rolling is sufficient to initiate the α→ω transition.

It follows from our experimental results that the transformation enthalpy $\Delta H_{Zr}^{\alpha\to\omega}$ is equal to -553 J/mol*, which is rather small. Thus, the increase in the driving force for cooling at 4K is also small. Therefore, in spite of the fact that the activation energy is also small ($\Delta F_{act}^{\alpha\to\omega}$ = 220 J/mol), the α→ω transformation process should not be completed even after such marked cooling. Hence the phase, while thermodynamically stable at $P=10^5$ Pa and T less than 200K, is present only in small amounts even after drastic cooling.

At the present time the only phenomenon which we cannot yet explain is that even when the pressure is very high and the driving force is 4 or 5 times greater than the activation barrier the transformations do not come to completion. However, it is clear that the elastic energy barrier is not sufficient to prevent the transformation process, because the volume changes which occur in the course of the transformation are small.

We have to mention in this point that we failed to observe in TEM the in pure Ti either cooled to 4.2K or pressurized up to 5.0 - 9.0 GPa. Therefore

---

* The enthalpy value $\Delta H_{Zr}^{\alpha\to\omega}$ can be calculated by use of the condition that $\Delta F_{Zr}^{\alpha\to\omega}$ at equilibrium line is zero and taking into account the new value of $\Delta S_{Zr}^{\alpha\to\omega}$ = -1.67 J/mol K.

$P_S^{\alpha \leftarrow \omega}$ in α-Ti is substantially higher than that for Zr in accordance with numerous literature data. Also, the titanium sponge which was used by us was not of spectroscopical purity as Zr and might be more contaminated by minor impurities and that has affected the $\alpha \to \omega$ transformation kinetic.

References

1. J.C. Jamieson, Science, 140, 72 (1963).

2. F. Bandy, G.E. Research Lab. Rept. N63-RL-3481C, Oct. 1963.

3. V.A. Zylbershteyn, G.I. Nosova and E.I. Estrin, Fiz. Metallor. i Metallovedenie 35, 584 (1973).

4. M.P. Usikov, V.A. Zylbershteyn, Phys. Stat. Sol. (a) 53 (1973).

5. G.A. Sargent, H. Conrad, Mat. Sci. Eng. 7, 220 (1971).

6. V.A. Zylbershteyn, N.P. Chistotina, A.A. Zharov. N.S. Grishina and E.I. Estrin, Fiz. metallov. metalloved. 39, 445 (1975).

7. L.V. Altshuler, A.A. Bakanova. Sov. Phys. Uspeki 11, 678 (1969).

8. A.I. Voropinov, G.M. Gandelman, G.M. Podvalui, Sov. Phys. Uspeki, 13, 56 (1970).

9. M.K. Koul, J.F. Breedis in "The Science, Technology and Application of Titanium". Ed. R.I. Yaffe, N.Y. p 817 (1970).

10. A.R. Kutzar, V.N. German, G.I. Nosova, Dokladi Acad. Sci. U.S.S.R. 213, 81 (1975).

11. D.D. Fontaine, R. Kikuchi, Acta Met. 22, N9, 1139, (1974).

12. J.C. Williams, B.S. Hickman, H.L. Markus, Met. Trans., 2, 1913 (1971).

13. A.W. Bouren. Scripta Met , 5, 709 (1971).

14. S.G. Fedotov in "Titanium Science and Technology" Plenum Press, V.2, p.871 (1973).

15. A.H. King, J.L. O'Brien, J.A. Roberts, P.R. Roberts, "Cryogenics" 5, 230 (1965).

16. V. Zwicker, R. Lohberg, W. Heller, Z. Metallkunder, 61, 836 (1970).

17. T.S. Luhman, R. Taggart, D.H. Polonis, Scripta Metall. 3, 777 (1969).

18. D. Kramer, G. Rodes, Trans. Met. Soc. AIME, 239, 1612 (1967).

19. T.H. Courtney, J. Wulfc, Mat. Sci. Eng., 4, 93 (1969).

20. N.S. Affonikooa, V.F. Degtiarova, V.A. Litvin, A.G. Rabinkin, Y.A. Skakov, Sov. Phys. Sol. State, 15, 875 (1973).

21. Ch. Leibovitch and A. Rabinkin, CALPHAD 4, 13 (1980).

22. L. Kaufman and H. Bernstein, Computer Calculations of Phase Diagrams, Academic Press, N.Y. and London, 1970.

23. L. Kaufman, Acta Met. 7, 575 (1959).

24. A. Gysler, W. Bunk and V. Gerold, Z. Metalkunde 65, 411 (1976).

25. R.M. Wood, Acta Met. 11, 907 (1963).

26. E.S. Fisher and D. Dever, Acta Met. 18, 265 (1970).

27 E.S Fisher and C.J. Renken, Physical Review 135, N21 (1964)

28. E.S. Fisher and M.H. Maughnani, J. Phys. Chem 32, 657 (1971).

29. B. Olinger and J.C. Jamieson, High Temp., High Pressures, 5, 123 (1973).

30. Ch Leibovitch, A. Rabinkin and M. Talianker, Met. Trans (in press)

31. D. de Fontaine, N. Paton and J. Williams, Acta Met. 19, 1153 (1971).

32. N.A. Vanderpuye, A.P. Miodownik "The Science Technology and Application of Titanium", ed. R.I. Yaffe and N.E. Promisel, Pergamon Press, p. 719, 1969.

33. P. Duwes, Trans ASM 45, 934 (1953).

34. K.K. McCabe and S.L. Sass, Phil. Mag. 23, 957 (1971).

35. E.K. Molchanova "Phase Diagrams of Titanium Alloys" ed. S G Glazunov, "Interpress, Jerusalem, 1965.

36. B.S. Hickman, J. Mater. Sci. 4, 554 (1960).

37. B.S. Hickman, J. Inst. Met. 96, 330 (1968).

38. R.G. Baggerly, Metallography, 8, 361 (1975).

39. B.S. Hickman, Trans. TMS AIME, 245, 1329 (1969).

40. B.D. Cullity: Elements of X-ray Diffraction 1st. ed. pp. 388-401, Addison-Wesley, Reading, Mass. 1956.

41. M.J. Blackburn and J.C. Williams, Trans. TMS-AIME, 239, 287 (1967).

42. Y.A. Bagaryatski, G.I. Nosova and T.V. Tagunova, DAH USSR, 122, 593 (1958).

43. G. Nosova, "Phasovie Previasheniva v titanovykh splavakh", Metallurgia, Moskva, 1969.

44. J.C. Williams and B.S. Hickman, Met. Trans. 1, 2648 (1970).

45. M.J. Blackburn and J.C. Williams, Trans. TMS AIME 239, 124 (1967).

46. J.M. Silcock, Acta Met. 6, 481 (1958).

47. S. Terauchi, H. Matsumoto, T. Sigimoto and K. Kamo (in Japanese). Preprint Faculty of Eng. Osaka Industrial University, Daito.

48. J.S. Williams, D. de Fontaine and N.E. Paton, Met. Trans. 4, 2701 (1973).

49. S.L. Sass, J. Less Common, Met. 22, 127 (1972).

50. L. Kaufman, Acta Met. 7, 575 (1959).

51. E. Estrin. Fiz Metal. Metaloved, 37, 1279 (1974).

52. J.O. Stiegler, J.T. Houston and M.L. Picklesimer, J. Nucl. Matls. 11, 32 (1964).

53. J.C. Williams and M.Y. Blackburn, Trans. TMS, AIME, 245, 2352 (1969).

54. M.J. Blackburn and J.C. Williams, Trans TMS, AIME, 242, 2461 (1968)

55. I.V. Lyasotsky and V.D. Tyapkin, Fis Metal. Metallov, 36, 1260 (1973).

56. N.N. Aparov, I.V. Lyasotskyi and V.D. Tyapkin, Fis Metalov, i metalloved 40, 1107 (1975).

57. Y.K. Vohra, Acta Met. 27, 1671 (1979).

58. E.W. Collings, J.C. Ho, Phys. Rev. B.1, 4289 (1970).

59. E.W. Collings, H.L. Gegel,"Physics of Solid Solution Strengthening", ed E.M. Collings, H.L Gegel, Plenum Press, N.Y. p 147

60. J.D. Fast, "Entropy". Philips Technical Library, 1962.

61 S. Weinig and E.S. Machlin, AIME Trans, 200, 1280 (1954)

62. F.C. Holden, H.R. Ogden and R.I. Jaffee. Trans. AIME, 206, 1388 (1956)

63 R.R. Zegfang and H. Conrad, Z. Metallkunde, 66, 422 (1975).

64. D.N. Williams, R.A. Wood and E.S. Bartlett, Metall. Trans. 3, 1529 (1972).

65 E. Levine, S. Hayden and H. Margolin, Acta Met. 22, 1443 (1974).

66. S.M. Tuominen and D.A. Koss. Mat, Sci Eng., 21, 71 (1975).

67. K.K. Sankaran, S.M.L. Sastry and P.S. Pao, Metall. Trans. 11a, 196 (1980).

68. A.W. Bowen, J. Mat. Sci. 12, 1355 (1977).

69. E.Y. Gutmanas, Scr. Met. 14, 269 (1980).

70. H. Scherer, D. Kohnlein, A. Rabinkin, W. Buckel (in publication).

71. Ch. Leibovitch, E. Gartstein and A. Rabinkin, Z. Metalkunde 71, 438 (1980).

72. F. Monkenaus, Diplomarbeit am Phys. Institut Universität Karlsruhe.

73. W. Gey and D. Köhnlein, Phys. Letters 29A, 450 (1969).

74. W. Gey and D. Kohnlein, Z. Physik 255, 358 (1972).

75. J.C. Ho and E.W. Collings, Physics of Ti-alloys I in Titanium Science and Technology. Edited by R.I. Jaffee and H.M. Burte, p. 815. Plenum Press, N.Y. 1973.

76. E.W. Collings, J.C. Ho and R.I. Jaffee "Physics of Ti-alloys II" in "Titanium Science and Technology" (Edited by R.I. Jaffee and H.M Burte) p. 831, Plenum Press, N.Y. 1973.

77. A. Eichler and W. Gey. Editions du CRNS, Grenoble, 1969.

78. P. Hohnberg, Diplomarbeit am Phys. Institut, Universitat, Karlsruhe

79. A. Eichler and J. Witting, Z. Angew. Physik, 25, 319 (1968).

80. W. Krah and D. Kohnlein, Z. Physik B 28, 19 (1977).

81. N.B. Brandt, N.I. Ginzburg, Sov. Phys. Uspekhi 8, 202 (1965).

82. A. Eichler and W. Gey, Z. Physik 251, 321 (1972).

83. A. Rabinkin, M. Talianker, O. Botstein, Acta Met. 29, 691 (1981).

84. O. Botstein, A. Rabinkin and M. Talianker, Scripta Met. 15, 151 (1981).

85. Itinosai, Proc. of II symposium on high pressures 24-26 Dec., 1969, Sendai, Japan.

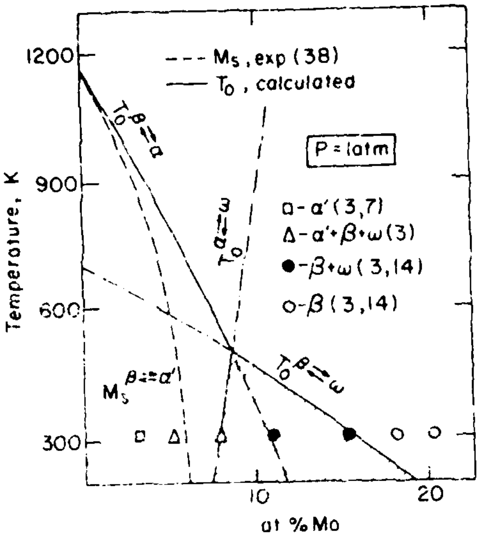

Fig.1. Computed T_0-x Diagram for Ti-Mo Alloys at One Atmosphere based on Equations (20),(23) and (24).

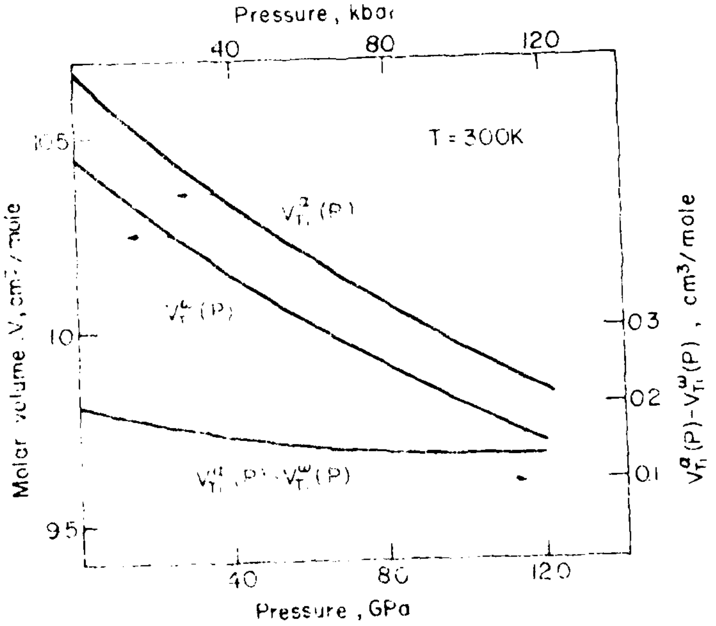

Fig.2. The volume of hcp and omega Titanium and the volume difference alpha minus omega for Titanium as a function of pressure at 300°K.

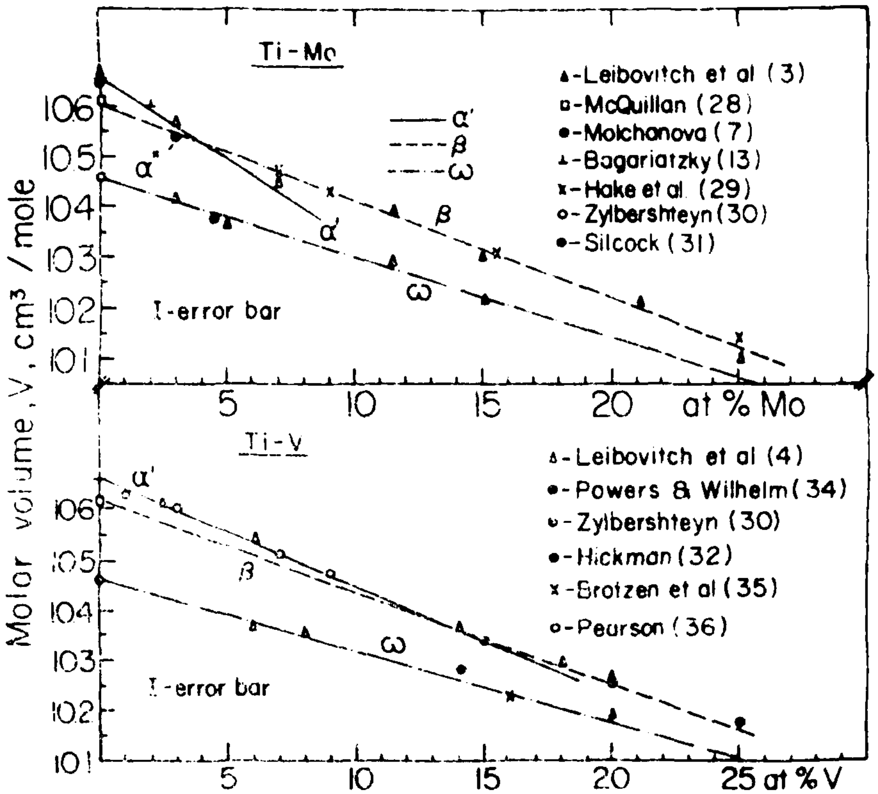

Fig.3. The molar volume of bcc(β) and omega (ω) structures in the Titanium-Molybdenum and Titanium-Vanadium Systems at one atmosphere and 300°K after various authors.

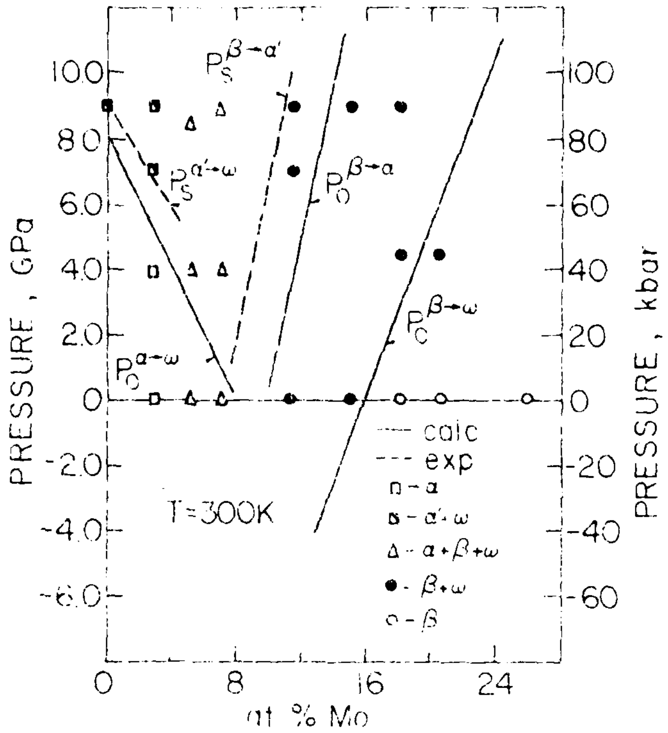

Fig.4. Summary of Experimental Data on Phase Stability of Ti-Mo Alloys (3,4) as a Function of Pressure at 300K Compared with Results Computed from Equations (34)-(36).

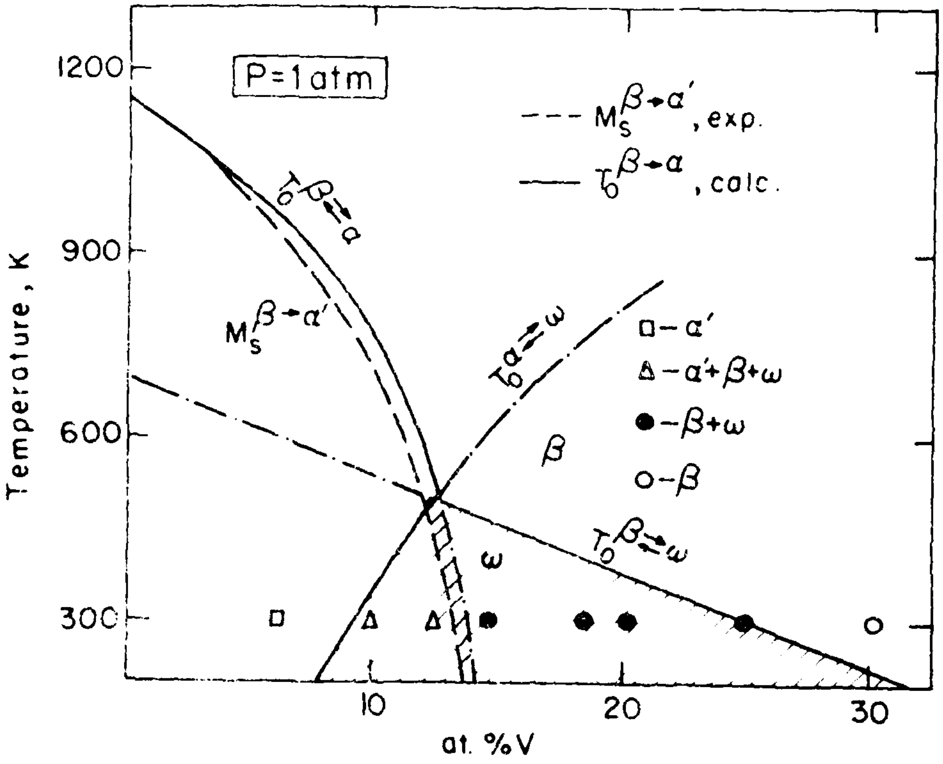

Fig.5. Computed T_0-x (m.d.e-metastable diffusionless equilibria) Diagram for Titanium-Vanadium Alloys Based on Equations (39) and (43,44).

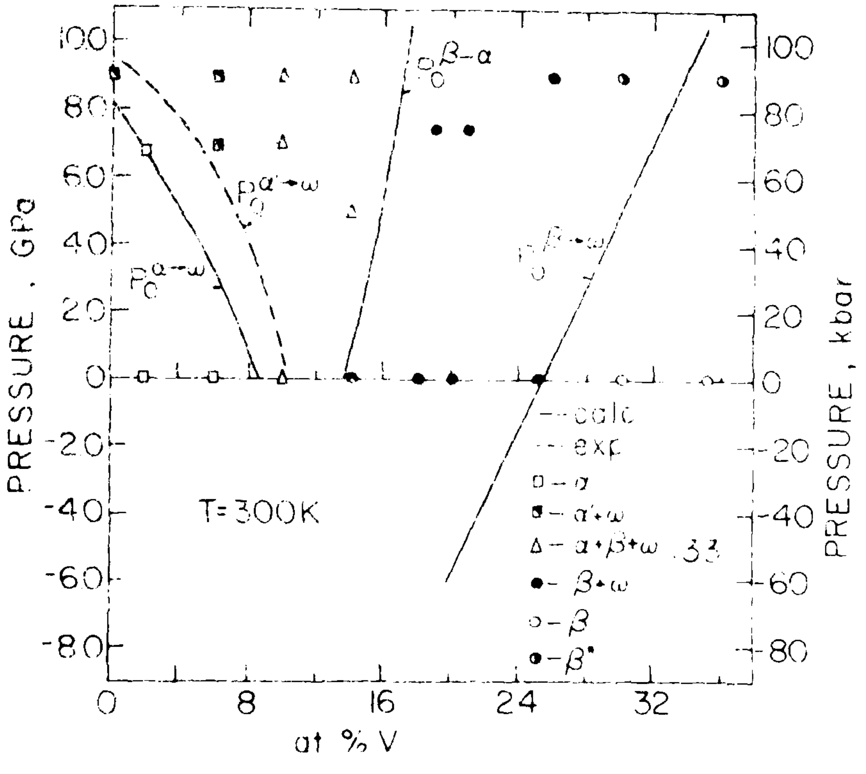

Fig.6. Computed 300K High Pressure m.d.e. Diagram for Ti-V alloys based on Equations (45)-(47) and Experimental Results on Phase Stability (33).

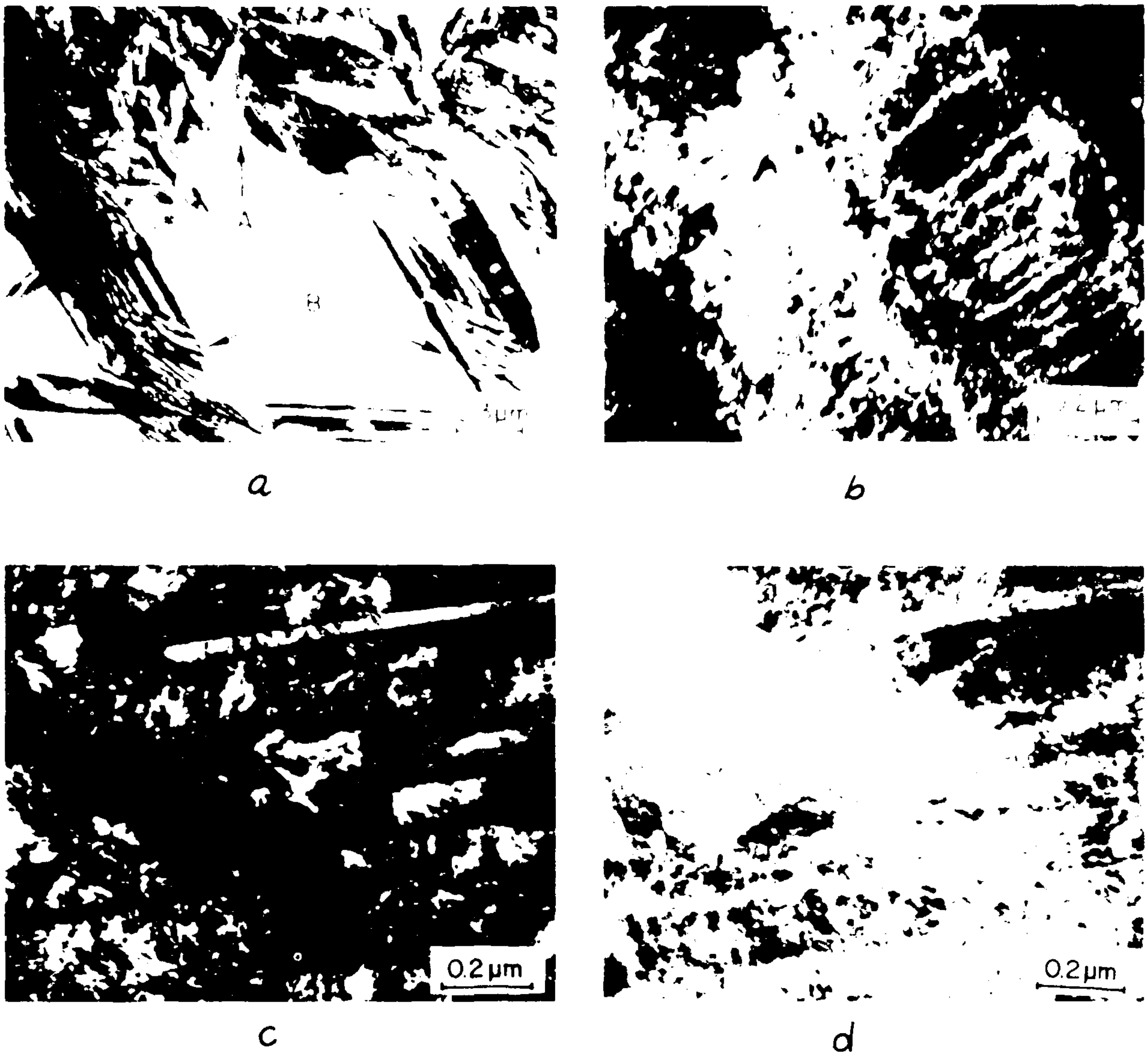

Fig.7: The structure of Ti-3% Mo Alloy.
a) TEM bright field micrograph, showing the complex martensitic structure in the as-quenched state. α' fine plates are seen in region (A) big plates of α' martensite (B) divide the bulk of what seems to be α'' martensite.
b) TEM dark field micrograph showing the small ω phase particles and dense dislocation network inside α' plates after hps 7.5 GPa.
c) TEM bright field micrograph after 9.2 GPa.
d) Pressure induced ω particles in the dark field of (c).

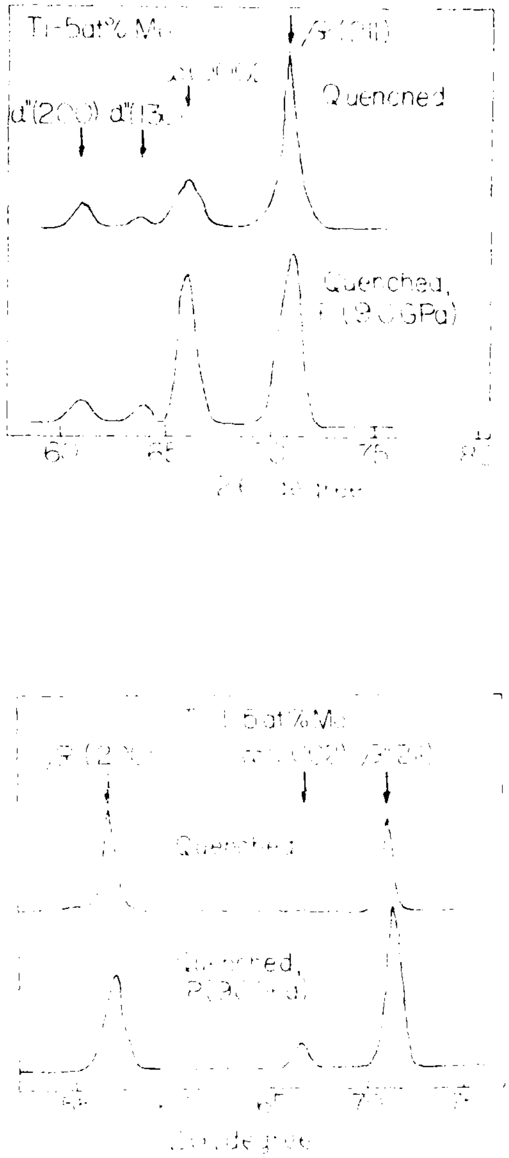

Fig. 8. X-ray diffractograms of Ti-Mo in the as-quenched state and after hps 9.0 GPa.

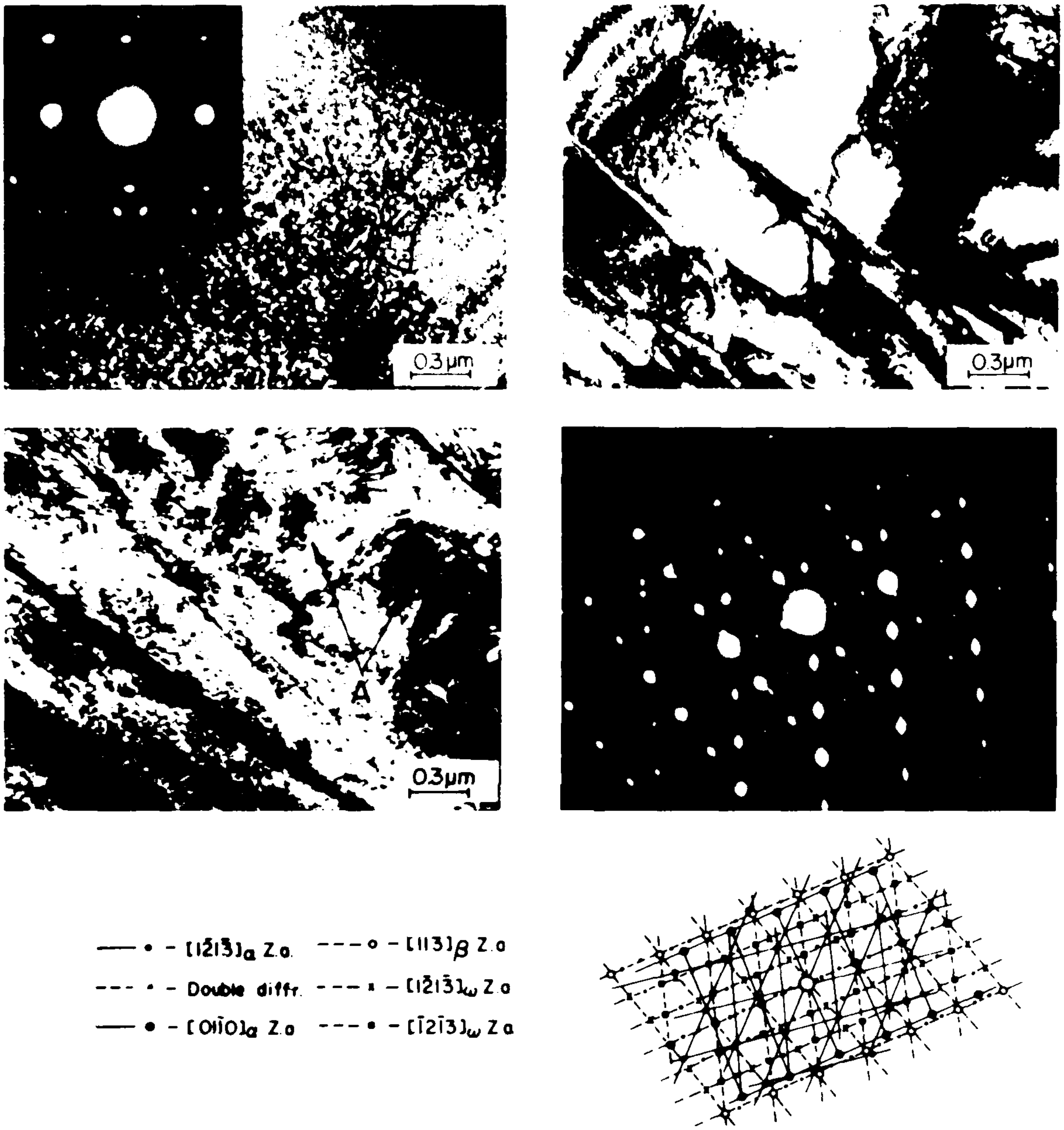

Fig. 9 The structure of Ti-5% Mo alloy. a) TEM micrograph of the as-quenched state, z.a.$[221]_{\beta}$. Fine ω particles and small α' martensite plates (A) are present in the β matrix. b) The TEM bright-field micrograph after hps 7.0GPa. The pressure-induced α' martensite plates grow at the expense of the β matrix. c) TEM dark-field micrograph after hps 9.0GPa. The large α' martensite plates contain ω+β mixture and "secondary" α' plate-like regions (A). d) Electron diffraction pattern of the region in Fig. 4c and e) the indexed scheme of the pattern in Fig. 4d.

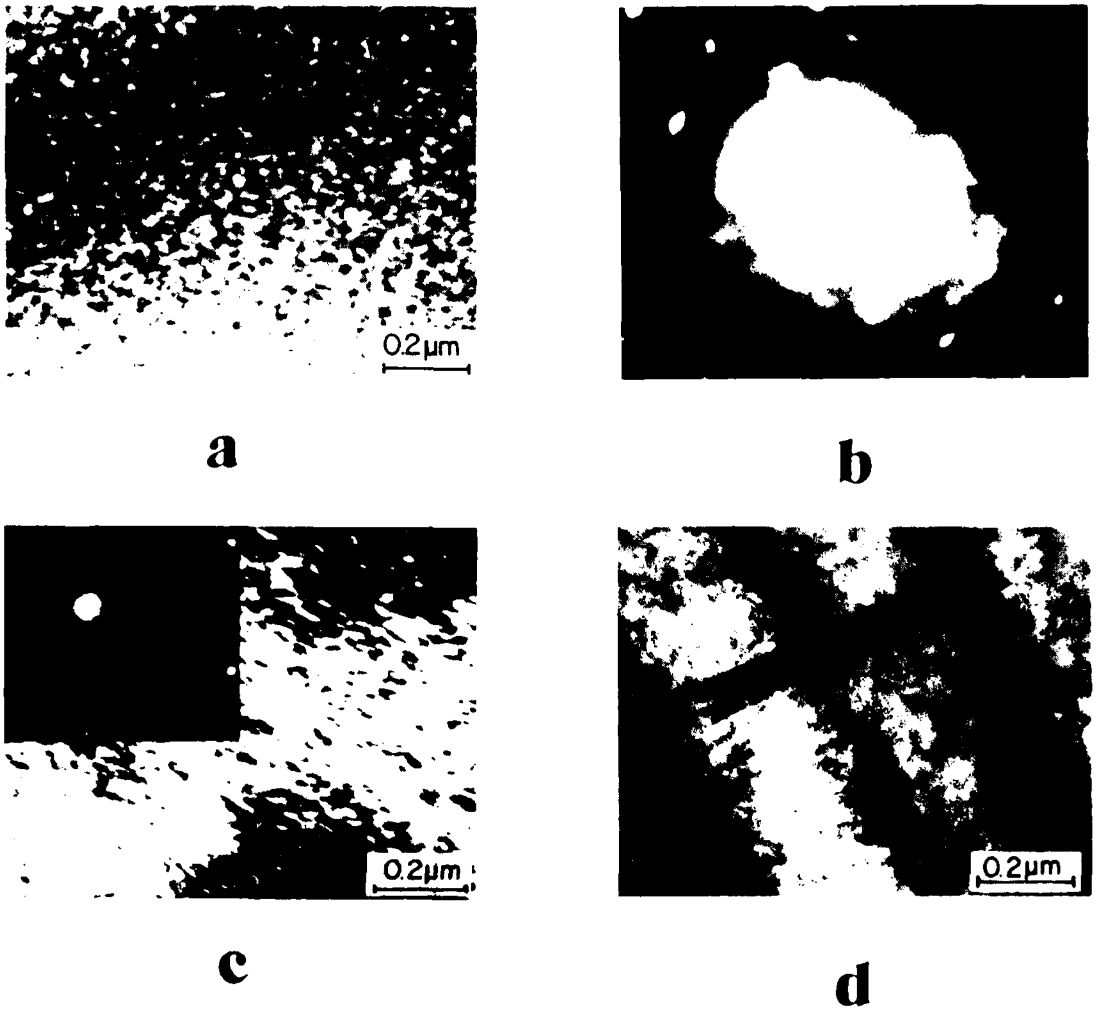

Fig. The structure of Ti-15 at.% Mo alloy. a) Dark field image and b) the corresponding electron diffraction pattern of the as-quenched state showing a complex network of diffuse intensity. Z.A.: $\sim[100]_{\beta}$ c) TEM dark field micrograph and electron diffraction pattern after hps 9.0 GPa. Z.A.: $[012]_{\beta}$. d) TEM bright field of the sample after hps 20 GPa. The pressure-induced α' martensite plates are clearly shown.

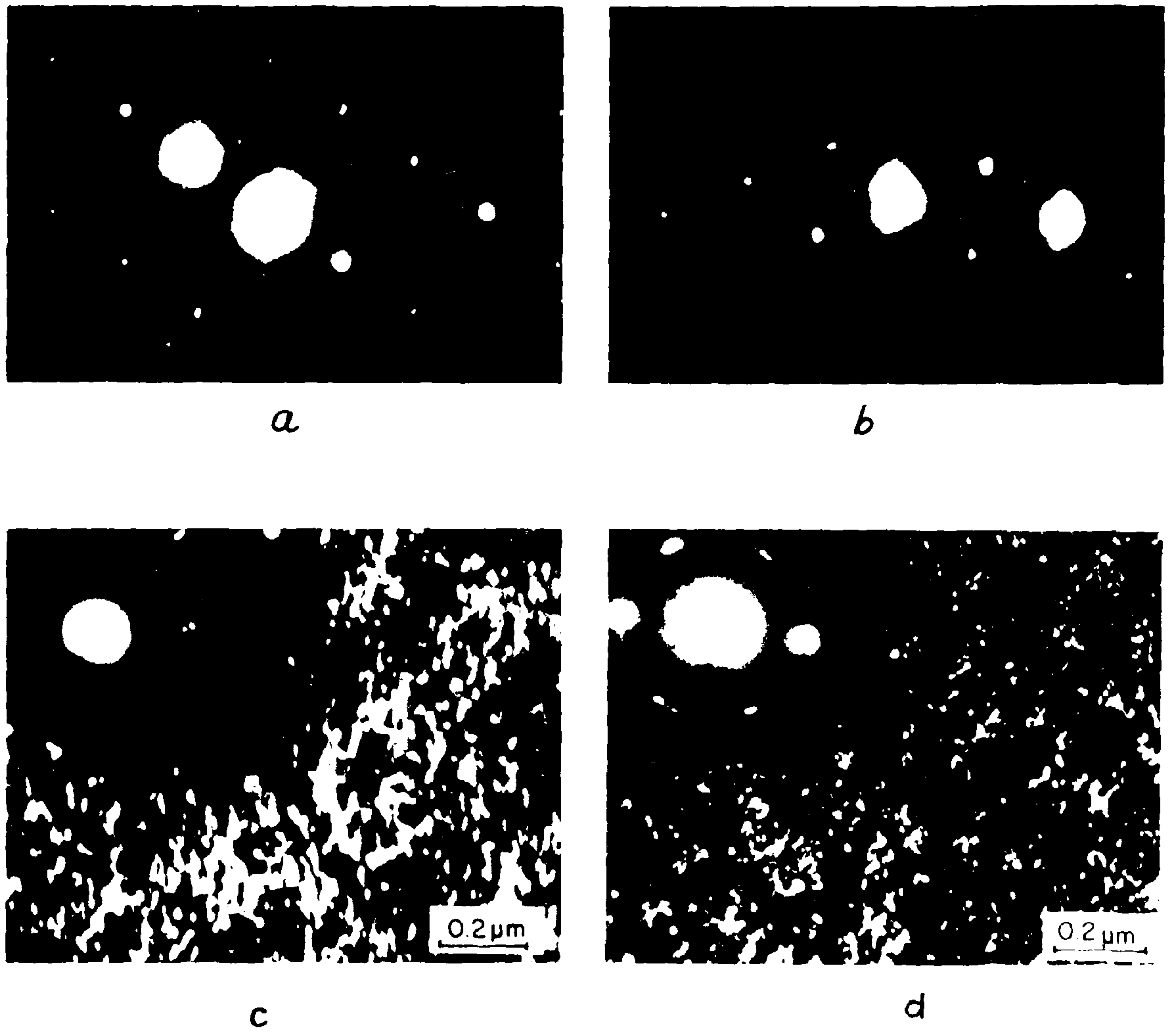

a b

c d

Fig.11 a) Diffuse scattering observed in the electron diffraction pattern of the as-quenched Ti-18% Mo alloy. b) Paired Kikuchi lines observed in the electron diffraction pattern of the as-quenched Ti-20% Mo alloy. TEM dark field micrographs of the c) Ti-18% Mo and d) Ti-25% Mo showing the particles of ω-like phase in the β matrix after hps 4.5GPa. Z.A. $[100]_\beta$ for Ti-18% Mo and Z.A. [[illegible]] for Ti-25% Mo.

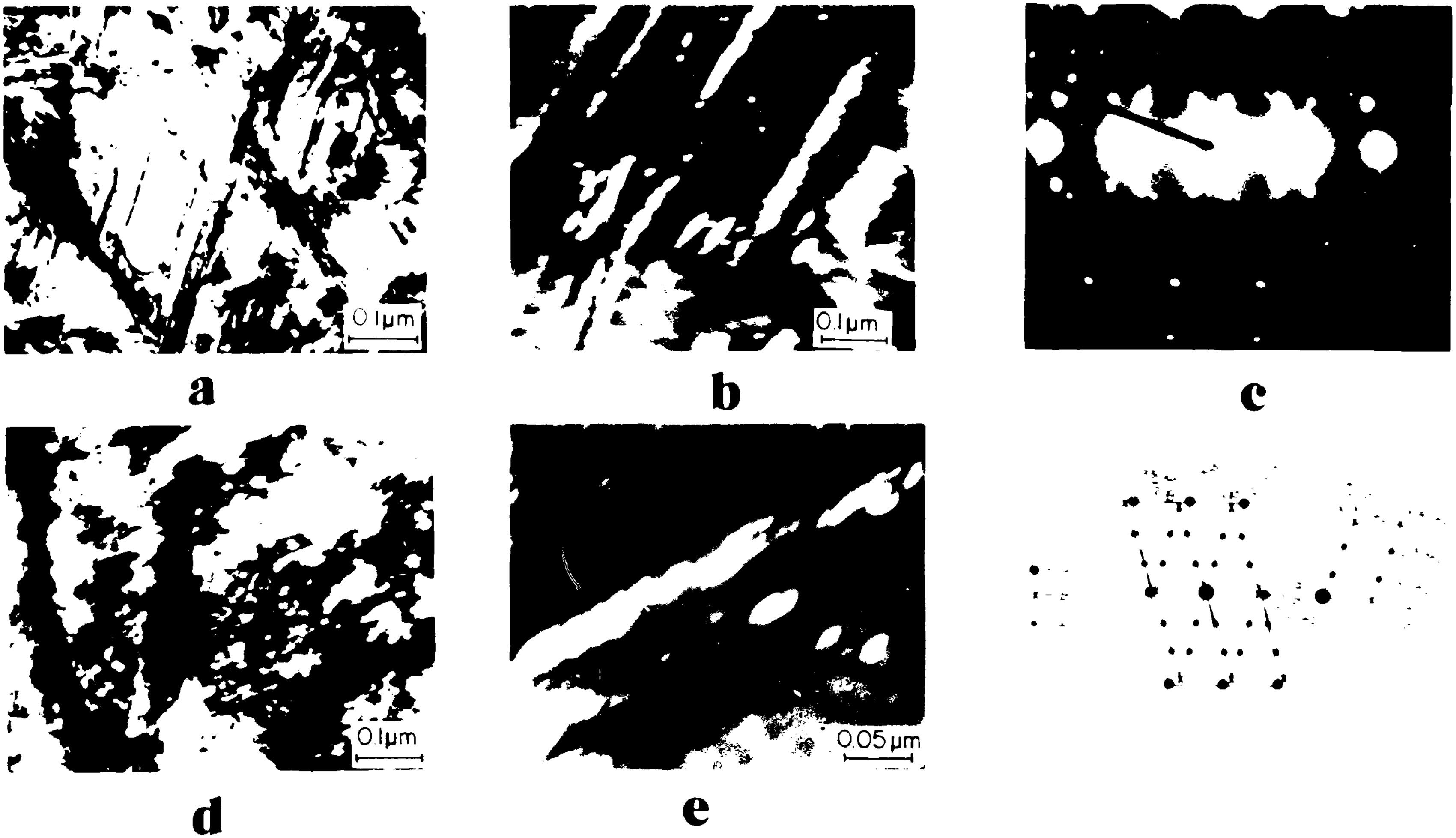

Fig. [illegible] microstructure of [illegible] as-quenched [illegible]
micrograph [illegible] of the same sample taken in [illegible] reflection [illegible]
contain fine particles. [illegible] SAD and [illegible] representation from the sample [illegible]
d) Dark field micrograph of [illegible] sample after [illegible] appear clearly [illegible]
e) [illegible] particles.

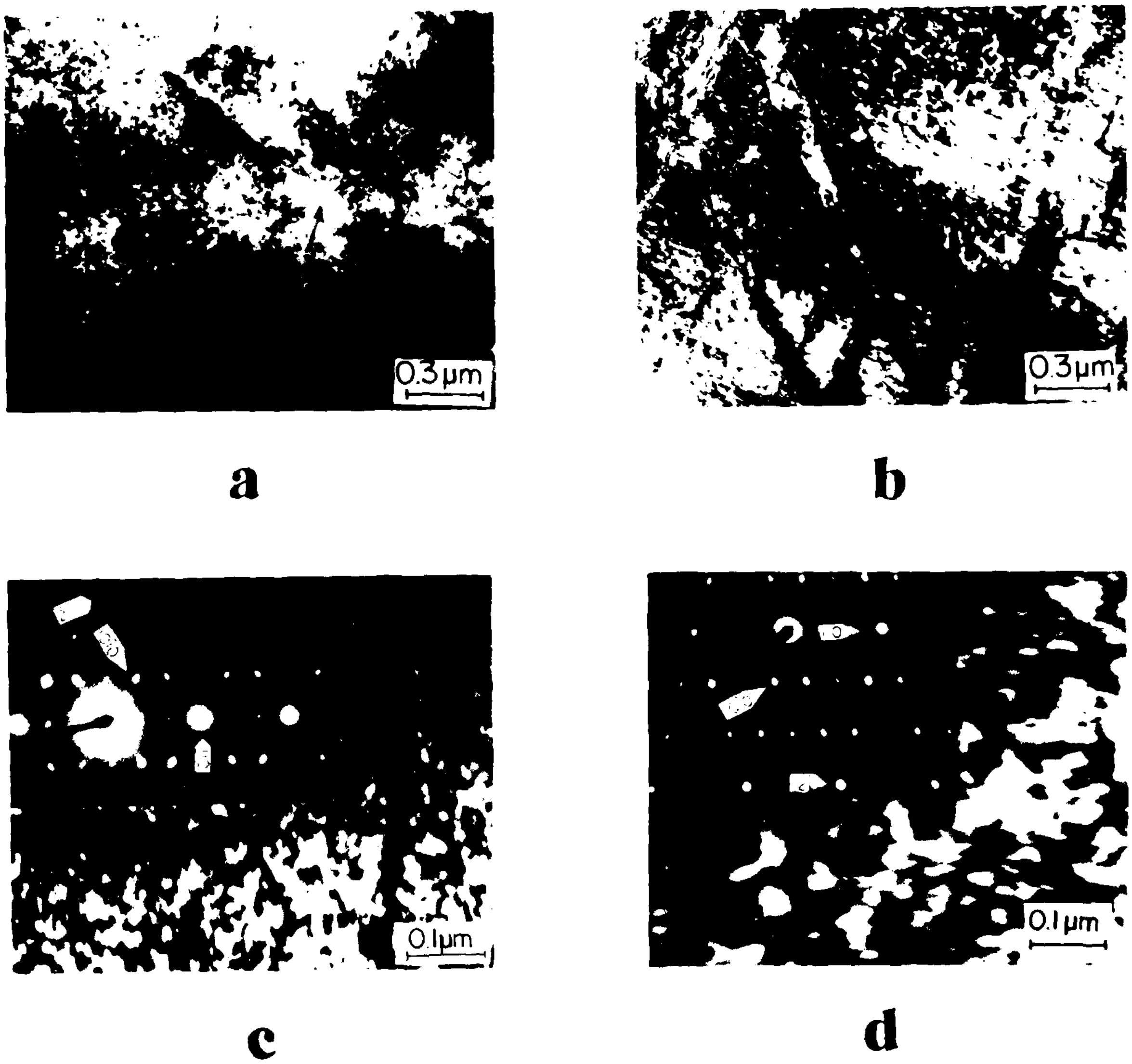

Fig. The structure of Ti-14 at.% V. alloy.
a) B.F. micrograph of the as-quenched state. Very fine ω-needles shown by arrows. b) B.F. of the same sample after 9.2 GPa. Substantial growth of ω-needles is clearly seen. c) Dark field of the as-quenched sample taken in ω reflex. (Inset: SADP with Z.A.:$[110]_{\beta}$).
d) D.F. of the same sample after 9.2 GPa. (Inset: SADP with Z.A.:$[113]_{\omega}$).

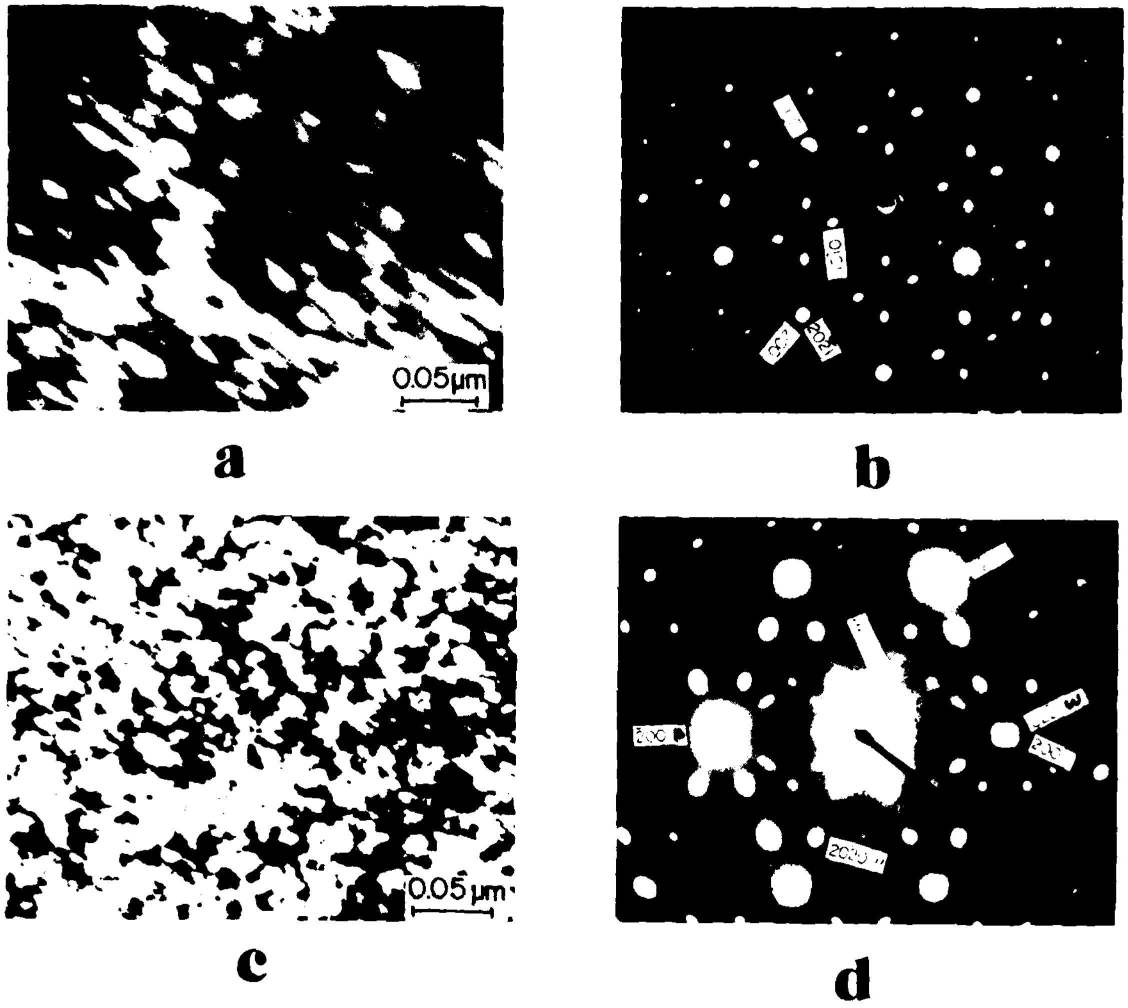

Fig. The structure of Ti-18 at.% V alloy. a) Dark-field micrograph taken from as-quenched state. b) Corresponding electron diffraction pattern. c) Dark-field micrograph taken after hps 9.2 GPa. d) Corresponding electron diffraction pattern.

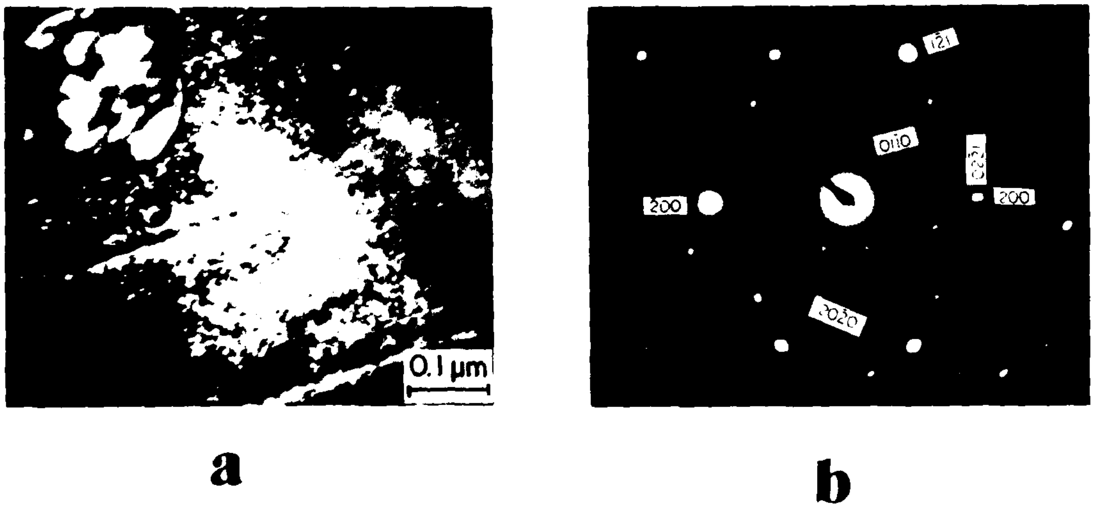

Fig. The structure of Ti-20 at.% V alloy after 7.5 GPa.
a) Dark field micrograph (Inset: Magnified circled place (x4). ω phase particles in β-matrix and needles of pressure-induced α phase are clearly seen. b) SADP of the sample Z.A.: $[012]_\beta$. 4-ω variants present: 2-with $[2\bar{1}\bar{1}\bar{6}]_\omega$ Z.A. and 2 with $[\bar{2}3\bar{1}2_\omega$ Z.A. which coincide with β reflections.

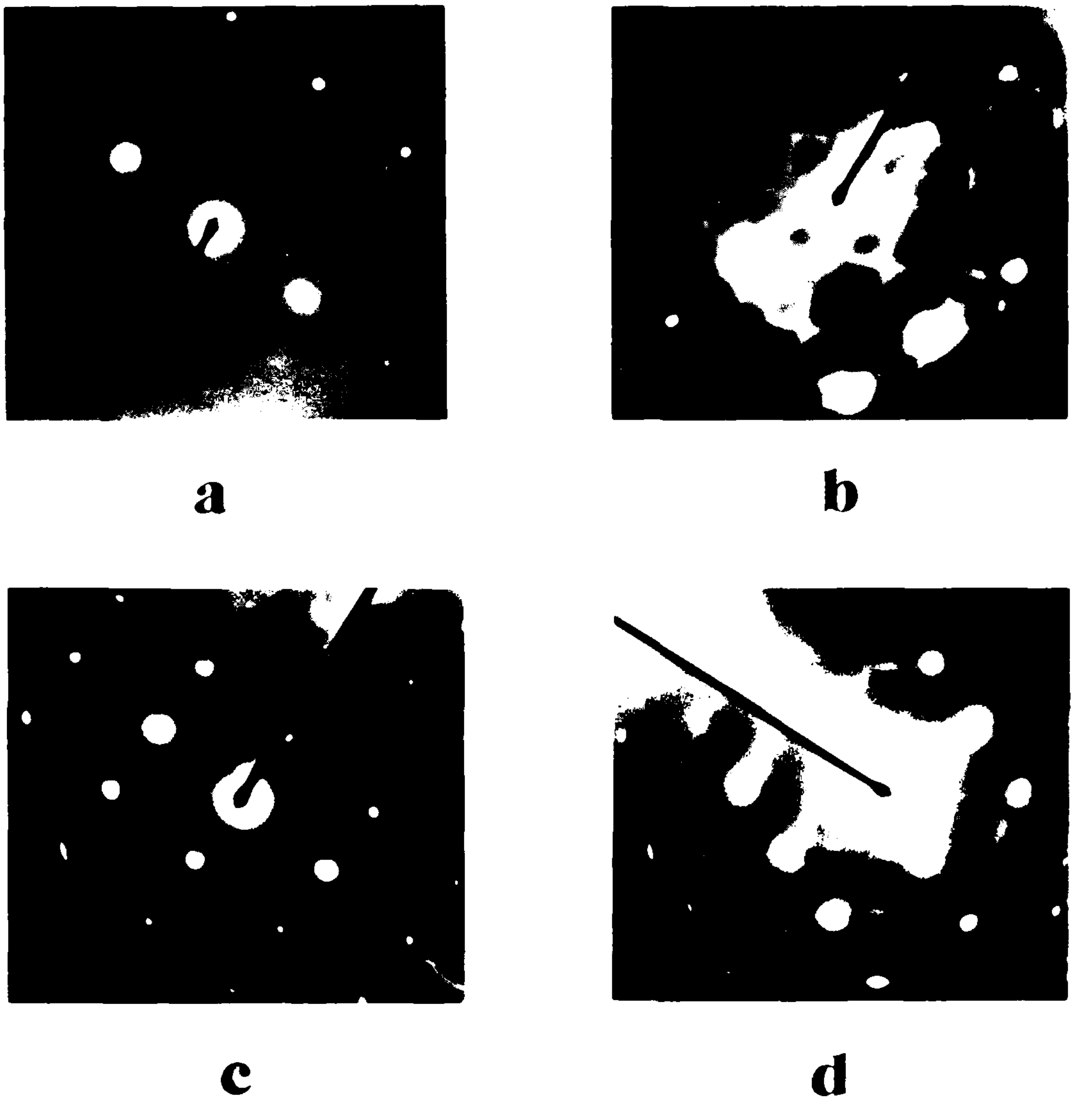
a
b
c
d

[illegible]

[illegible]

[illegible]

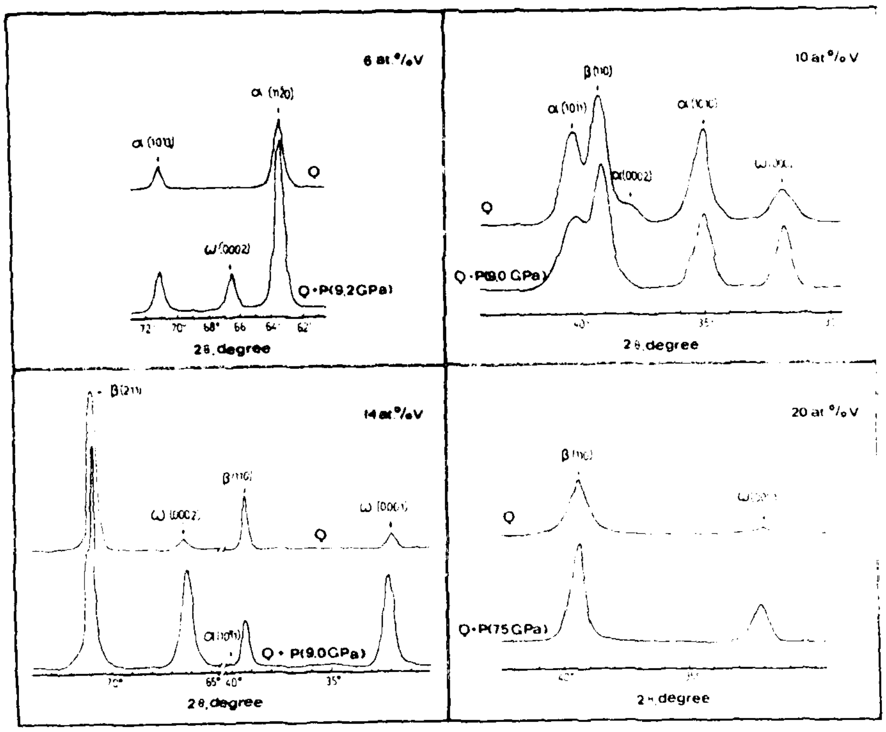

Fig. 17. X-ray diffractograms of as-quenched (Q) Ti-V alloys and alloys that were initially quenched and then peressurized (Q+P). Diffr. patterns were taken at atmospheric pressure.

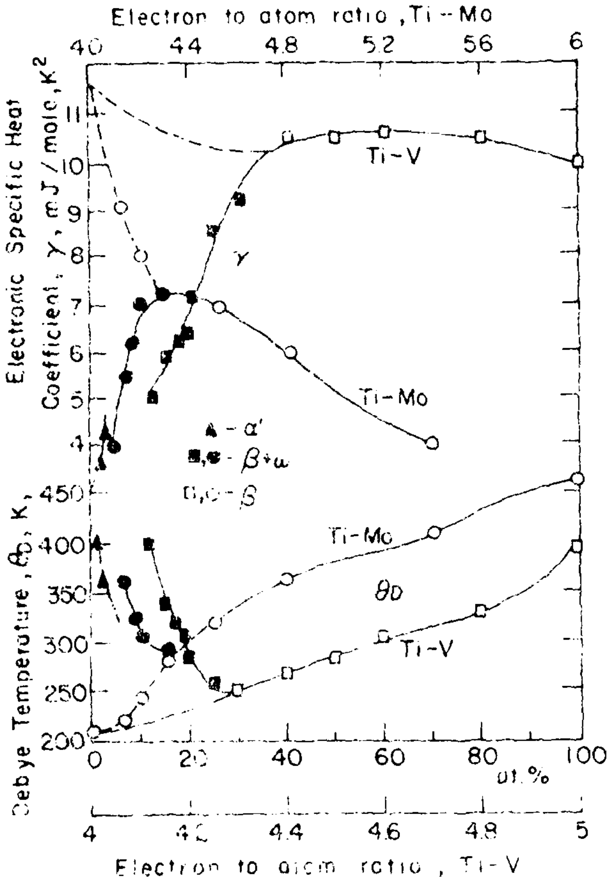

Fig.18. Debye temperature and electronic specific heat coefficient of Ti-V and Ti-Mo alloys [58,59].

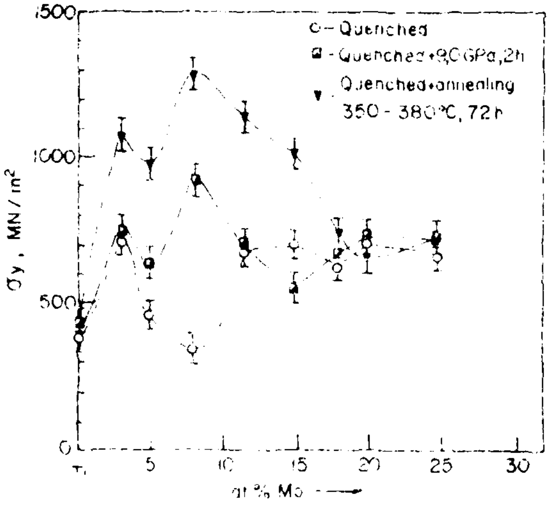

Fig.19. Yield Stress, σy, as a function of composition in Ti-Mo alloys after various treatments: 0-quenched, ■ -quenched + hps 9.0 GPa and ▼-quenched + thermal treatment (350°-380°C, 72h).

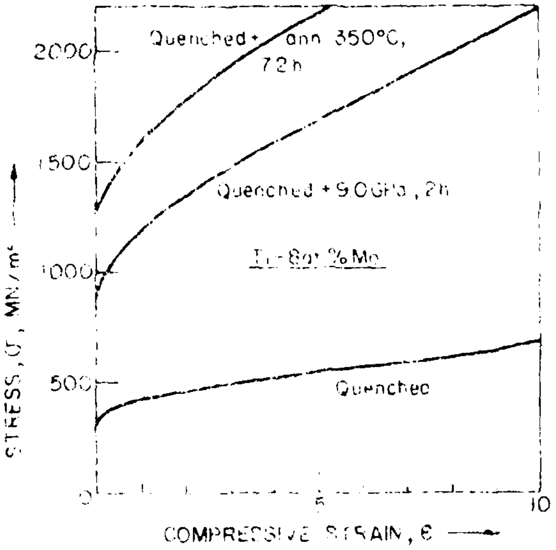

Fig.20 Stress-strain curves for Ti-8% Mo after various treatments: as-quenched, quenched + hps 9.0 GPa and quenched + annealed (350°C, 72 h).

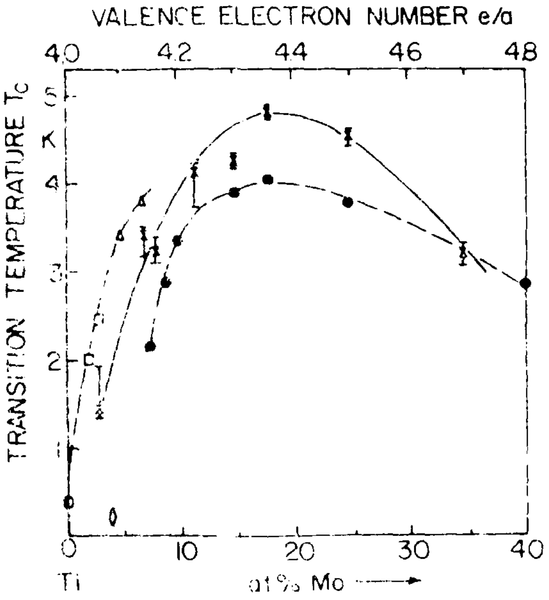

Fig.21. Transition temperature of Ti-Mo-alloys

x present work
O, , Δ : α, α' and α" - phases
O, β-phase, -phase, J.C. Ho and E.W. Collings

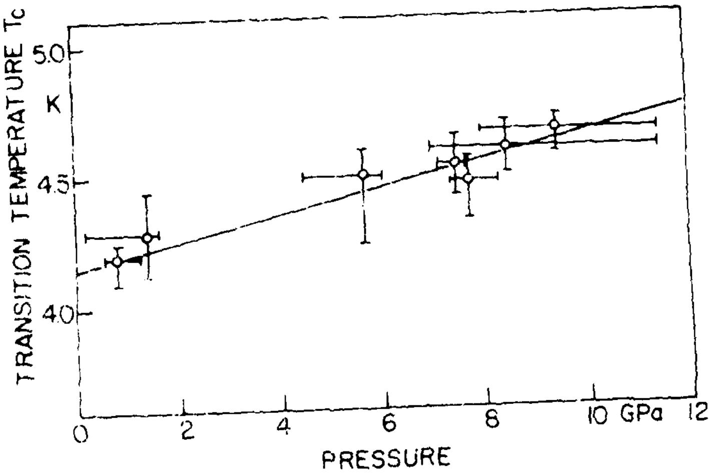

Fig.22a. Transition curves of Ti + 11.5 at% Mo under pressure.

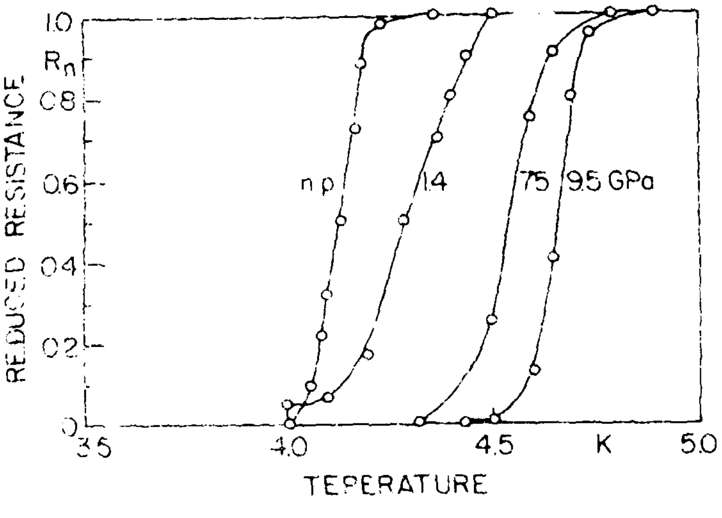

Fig.22b. Transition temperature of Ti + 11.5 at% Mo as a function of pressure.

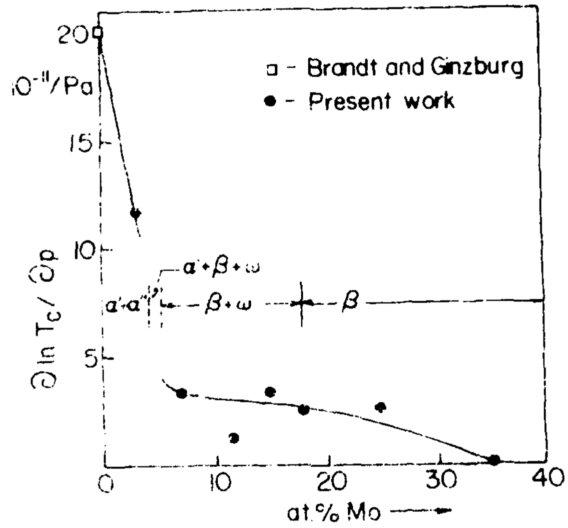

Fig.23. Reduced pressure effect ln T_c/ p of Ti-Mo-alloys as a functin of Mo-concentration.

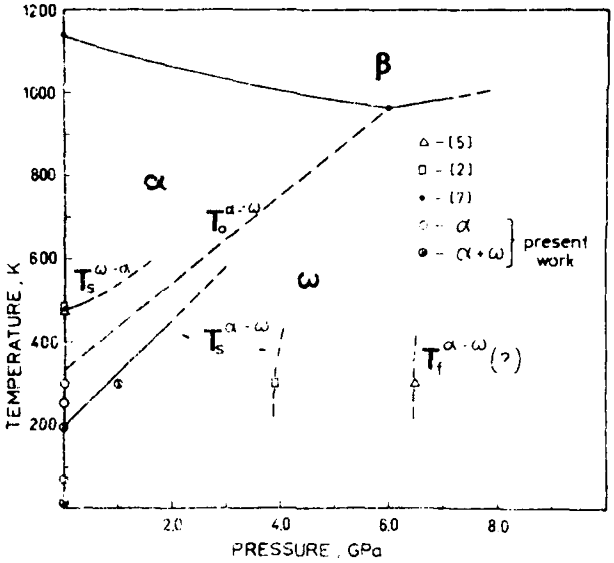

Fig.24. T-P diagram for Zirconium.

END

DATE
FILMED

7-81

DTIC